EYE-CLIMA
Verifying emissions of climate forcers

Updated high-resolution fluxes and uncertainties of CO_2, CH_4 and N_2O for Europe

DELIVERABLE 2.4

Author(s):	Tuula Aalto, Philippe Peylin, Almut Arneth, Jianyong Ma, Tiina Markkanen, Antti Leppänen, Vladislav Bastrikov, Elodie Salmon
Date of submission:	26-02-2026
Version:	1.0
Responsible partner:	FMI
Deliverable due date:	31-12-2024
Dissemination level:	Public

Call:	HORIZON-CL5-2022-D1-02
Topic:	Climate Sciences and Responses
Project Type:	Research and Innovation Action
Lead Beneficiary:	NILU - Norsk Institutt for Luftforskning

This project has received funding from the European Union's Horizon Europe research and innovation programme under grant agreement No 101081395

Document History

Version	Date	Comment	Modifications made by
0.1	09-02-2026	First Draft	Tuula Aalto, Philippe Peylin, Almut Arneth, Jianyong Ma, Tiina Markkanen, Antti Leppänen, Vladislav Bastrikov, Elodie Salmon
0.2	12-02-2026	Internal review	Audrey Fortems-Cheiney
0.3	26-02-2026	Final version	Tuula Aalto, Philippe Peylin, Almut Arneth, Jianyong Ma, Tiina Markkanen, Antti Leppänen, Vladislav Bastrikov, Elodie Salmon
1.0	26-02-2026	Submitted to Commission	Rona Thompson

This project has received funding from the European Union's Horizon Europe research and innovation programme under grant agreement No 101081395

Summary

The primary objective of this deliverable is to provide policy relevant estimates of major GHG fluxes: CO_2 (see Section 2), N_2O (see Section 3), and CH_4 (see Section 4) from process-based models. The bottom-up flux estimates are derived at high spatial resolution (~10 km) over Europe to be used in: 1) gridded flux estimates for prior information in the atmospheric inversions in WP3, and 2) national and sub-national annual GHG budgets for the synthesis in WP4 and 3) providing data for improving the understanding of key drivers for each GHG land flux and the impacts of ecosystem management (e.g. for crops, grasslands and forests) to the net annual fluxes in comparison to other drivers such as climate, atmospheric CO_2 and nitrogen deposition. Three ecosystem modelling frameworks are used to estimate the emissions: 1) LPJ-GUESS which is used to estimate the net ecosystem exchange (NEE) of CO_2 and soil N_2O emissions across natural, pasture, and crop ecosystems, 2) JSBACH-HIMMELI for estimating wetland, mineral soil and inundated land CH_4 emissions, and 3) ORCHIDEE which is used to estimate emissions of all three greenhouse gas components, CO_2, CH_4 and N_2O, from the European ecosystems.

Note that some of these data may be password-protected during a consolidation phase and thus only accessible to the EYE-CLIMA partners. However, after this phase, all data will be published in the Zenodo data repository and made available to everyone.

This project has received funding from the European Union's Horizon Europe research and innovation programme under grant agreement No 101081395

TABLE OF CONTENTS

This project has received funding from the European Union's Horizon Europe research and innovation programme under grant agreement No 101081395

1. Introduction

The objective of EYE-CLIMA deliverable D2.4 is to provide estimates of major GHG fluxes (CO_2, CH_4, and N_2O) from process-based models. The bottom-up flux estimates will be derived at high spatial (~10 km) and 3-hourly or daily temporal resolutions (depending on the model) over Europe to be used in: i) gridded flux estimates (with quantified uncertainties) for prior information in the atmospheric inversions in WP3, and ii) national and sub-national annual GHG budgets for the synthesis in WP4. Two state-of-the art models have been selected for each GHG, including one with multiple data-stream assimilation for CO_2. The models will help to assess the contribution to GHG fluxes from ecosystem subcomponents, such as above-ground versus below-ground, the split between different ecosystem types (forest, natural grassland, crops, peatland, etc) which will help to develop GHG reduction strategies. The data presented in this report are the final versions and are an update to the earlier versions presented in D2.3.

2. Process modelling of LULUCF sector CO_2 fluxes for Europe

2.1 ORCHIDEE

Overall model description

ORCHIDEE (Organizing Carbon and Hydrology In Dynamic Ecosystems) is the Land Surface component of the Earth System Model - ESM from the Pierre Simon Laplace Institute (IPSL-CM6). It represents the dynamics governing the water, carbon, nitrogen, and energy balances of land ecosystems, following a process-based approach as much as possible. The modelling structures concentrates on several aspects: the exchanges of energy and water between the atmosphere and the biosphere and the carbon cycle dealing with photosynthesis, carbon allocation, litter decomposition, soil carbon dynamics, maintenance and growth respirations, plant phenology (Krinner et al., 2005) and a recent inclusion of carbon-nitrogen interactions (Zaehle and Friend, 2010; Vuichard et al., 2019).

The vegetation heterogeneity is described using fractions of 15 different plant functional types (PFTs) for each grid cell. All PFTs share the same equations but with different parameters, except for the leaf phenology. The annual evolution of the PFT maps (including a wood harvest product) is derived from the LUHv2 database (Lurton et al., 2020). In each grid cell, the PFTs are grouped into three soil tiles according to their physiological behaviour: high vegetation (forests) with eight PFTs, low vegetation (grasses and crops) with six PFTs, and bare soil with one PFT. An independent hydrological budget is calculated for each soil tile, to prevent forests from exhausting all soil moisture. In contrast, only one energy budget (and snow budget) is calculated for the whole grid cell. All components of the surface energy and water budgets, as well as plant/soil carbon fluxes, are computed at a sub-daily time step (i.e. 30 min) using a standard “big leaf” approach, but the “slow” processes (carbon allocation in the different plant reservoirs and litter and soil carbon dynamic) are computed on a daily time step. A physically based 11-layer soil hydrology scheme is used and vertical water fluxes are described using the Richard equation discretized with 11 layers for a 2 m soil depth, and a free drainage condition is imposed at the bottom of the soil column (de Rosnay et al., 2002; D'Orgeval et al., 2008). As detailed in Wang et al. (2016), the vertical discretization for heat diffusion is identical to that adopted for water up to 2 m. Furthermore, the soil depth for heat diffusion is extended to 90 m, with a zero-flux condition at the bottom and 18 calculation nodes. Finally, a three-layer snow scheme of intermediate complexity described in Wang et al. (2013) is included.

For the carbon cycle, photosynthesis depends on light availability, CO_2 concentration, soil moisture, and surface air temperature. It is parameterized based on Farquhar et al. (1980) and Collatz et al. (1992) for C_3 and C_4 plants, respectively. We used the implementation proposed by Yin and Struik (2009) that derives an analytical solution of the three equations linking the net assimilation rate, the stomatal conductance, and the intercellular CO_2 partial pressure. Once the carbon is fixed by photosynthesis, we

This project has received funding from the European Union’s Horizon Europe research and innovation programme under grant agreement No 101081395

compute the autotrophic respiration (growth and maintenance) and then allocate the remaining carbon into eight plant compartments (below and above ground sapwood and heartwood, leaves, fruit, roots, and reserves). Each compartment has a specific turnover depending on environmental stresses, and the living biomass is turned into a litter pool that is distributed in four compartments (metabolic or structural, both above or below ground). The litter is decomposed following first-order kinetics equations, modulated by upper soil moisture and temperature, with a fraction that is respired and a fraction that is distributed into three soil organic carbon pools (active, slow, and passive), following the CENTURY model (Parton et al., 1987). Each soil organic carbon pool is also decomposed following first-order kinetic equations modulated by soil moisture and temperature. Overall, the carbon respired from the litter and soil carbon pools defines the heterotrophic respiration.

Model version and configuration for EYE-CLIMA simulations

The model version that is used for the project (including for the prior of the atmospheric inversions and for the synthesis) is the one including the nitrogen cycle (ORCHIDEE-V3), which was described in Vuichard et al., (2019). This version is also the one that was used in the last two TRENDY model intercomparison for the global carbon budget (Friedlingstein et al., 2022). Key features of this version are:

- The nitrogen cycle, like the carbon cycle, is included at the PFT level.
- There is a parallel nitrogen pool for each carbon pool, with carbon to nitrogen (C:N) ratios varying throughout time.
- The C:N ratio at the leaf level varies as a result of nitrogen supply by roots and biomass allocation requirement.
- The C:N stoichiometry of the remaining live biomass pools (belowground and aboveground sapwood, belowground and aboveground heartwood, fruit, and fine roots) is determined by the C:N ratio of the leaves but multiplied by a pool-dependent factor *fcn*.
- In terms of the Soil Organic Matter (SOM) decomposition, ORCHIDEE follows the scheme in which C/N ratios of SOM pools are expressed as a function of soil mineral nitrogen content (ammonium and nitrate).

More details on the nitrogen cycle with respect to the emissions of N_2O fluxes are provided in Section 3.

The model is run for Europe with a dedicated forcing, prepared specifically for the project (see deliverable D2.2), and updated for this last set of simulations: a product based on the ERA5-land climate reanalysis of ECMWF (European Centre for Medium-Range Weather Forecast) with a bias correction using the Climate Research Unit (CRU) monthly dataset, at the spatial resolution of around 11 km. The simulations follow a protocol similar to the TRENDY protocol (Friedlingstein et al., 2022) but adapted for Europe. The model spin-up (procedure used to bring carbon pools to equilibrium) is performed by recycling the first 20 years of available atmospheric forcing (1901-1920) over the 340 years long simulation with the CO_2 atmospheric concentration fixed to pre-industrial level (276.59 ppm, corresponding to the year 1700). PFT and land-use maps and nitrogen inputs were prepared accordingly. The transient simulation is run for the years 1700-1900, still recycling the same forcing (1901-1920), but changing the CO_2-level and other inputs accordingly. Finally, the historical simulation is performed for 1901-2022 with time varying input data.

A data assimilation tool, ORCHIDAS, (https://orchidas.lsce.ipsl.fr/) has been used to optimize key parameters of the ORCHIDEE model using carbon- and nitrogen-related in-situ observations (eddy covariance and chambers). The system allows the optimization of selected parameters with multiple data streams, taking into account the different sources of uncertainty (parameter, model, observation) through a Bayesian framework. This version was optimized using carbon flux data collected on sites from the FLUXNET network. In addition, we have used manipulation experiment data from two Free Air

This project has received funding from the European Union's Horizon Europe research and innovation programme under grant agreement No 101081395

CO_2 Enrichment (FACE) experiments, to provide further constraints on vegetation response to increasing CO_2 by assimilating data under ambient and elevated CO_2 conditions. We found that we were able to improve the magnitude of modelled productivity simulated by this model version (Raoult et al., 2024).

Main results for CO_2 fluxes

A few results are presented below to illustrate the Net Biome Production (NBP) and the Gross Primary Production (GPP) simulated by ORCHIDEE over Europe. Figure 2.1.1 shows the spatial distribution of both NBP and GPP over the last decade. The spatial distribution of the GPP provides higher spatial heterogeneity following different climate conditions, nitrogen deposition and PFT distributions, while the NBP has a smoother spatial pattern. Overall, the western central part of Europe seems to have the largest carbon uptake. The highest GPP values seem to occur close to highly industrialised regions, where the nitrogen deposition and fertilisation are the highest.

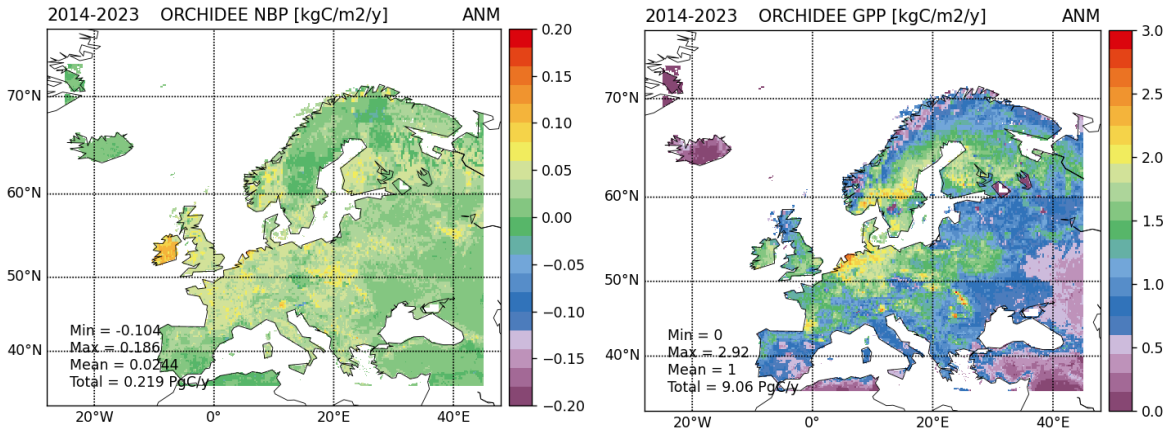

Figure 2.1.1: *Maps of simulated CO_2 fluxes from ORCHIDEE over Europe averaged over 2014 to 2023. Left: net biome production (net CO_2 flux including flux from harvested products) with positive flux indicating a C sink and right: Gross Primary Production (GPP) with positive flux indicating a C uptake.*

We then looked at the temporal evolution of the NBP (Figure 2.1.2) and the total values for the EU27+3 (UK + Switzerland + Norway) in Table 2.1.1. Large variations of the annual NBP occur for all forest, grassland and cropland ecosystems over the period 2000 - 2023. For the forests, variations between 30 and 110 TgC/yr are visible with very low carbon uptake in 2000, 2006, 2018 and 2022. These correspond mainly to drought conditions in Europe and large heat waves. Conversely, we observe large C uptake during 2002, 2007-2009 and 2020-2021. For grassland, the variations range between 0 and 150 TgC/yr with more variation in the second decade (2010-2020) than the first decade (2000-2010) of the simulation. The years with low NBP for grasslands do not correspond to the same years as for the forests, indicating different drivers of the NBP for grassland. We also tend to see a decreasing trend of NBP over this period (less C uptake). For cropland, NBP oscillates between large carbon uptake (up to 100 TgC/yr) and a few years with negative NBP (a positive carbon flux to the atmosphere) up to -75 TgC/yr. The total NBP flux is on average a land carbon sink around 200 TgC/yr except for the year 2022 (-50 TgC/yr).

This project has received funding from the European Union's Horizon Europe research and innovation programme under grant agreement No 101081395

Table 2.1.1: *Total net biome production (net ecosystem exchange including also the harvest products; NBP TgC yr^{-1}) simulated by ORCHIDEE in forest, grassland, and cropland for EU27+3 (UK + Switzerland + Norway) countries between 2000-2022. Negative values indicate C uptake.*

Year	Forest TgC yr^{-1}	Grassland TgC yr^{-1}	Cropland TgC yr^{-1}	Total TgC yr^{-1}
2000	-30.7	-116.5	0.5	-146.8
2001	-81	-123.5	-49.7	-254.2
2002	-100.1	-86.3	-65	-251.4
2003	-49.6	-103.6	69.7	-83.4
2004	-92.5	-103.3	-109.2	-305
2005	-36.9	-128.9	-12	-177.7
2006	-24	-80	-21.5	-125.5
2007	-108.2	-44	-74.9	-227.1
2008	-112.5	-81.7	-5.9	-200.1
2009	-104	-166.8	21.6	-249.2
2010	-81.3	-163.4	-68.7	-313.4
2011	-49.8	-11.9	-1.9	-63.5
2012	-54.3	-96.4	11.7	-138.9
2013	-72.4	-69.7	-57.1	-199.2
2014	-103	0	-64.6	-167.6
2015	-77.2	-92.2	41	-128.4
2016	-79.1	-70.7	-43.4	-193.2
2017	-41.2	-141	-36.9	-219
2018	-24.4	-1.1	12.7	-12.8
2019	-50.1	-91	-3.2	-144.3
2020	-86.5	-6.7	-48.2	-141.3
2021	-92.7	-199.4	-61.1	-353.2
2022	-28.9	10.9	87.5	69.4
2023	-65.9	-45.1	-63.8	-174.9

This project has received funding from the European Union's Horizon Europe research and innovation programme under grant agreement No 101081395

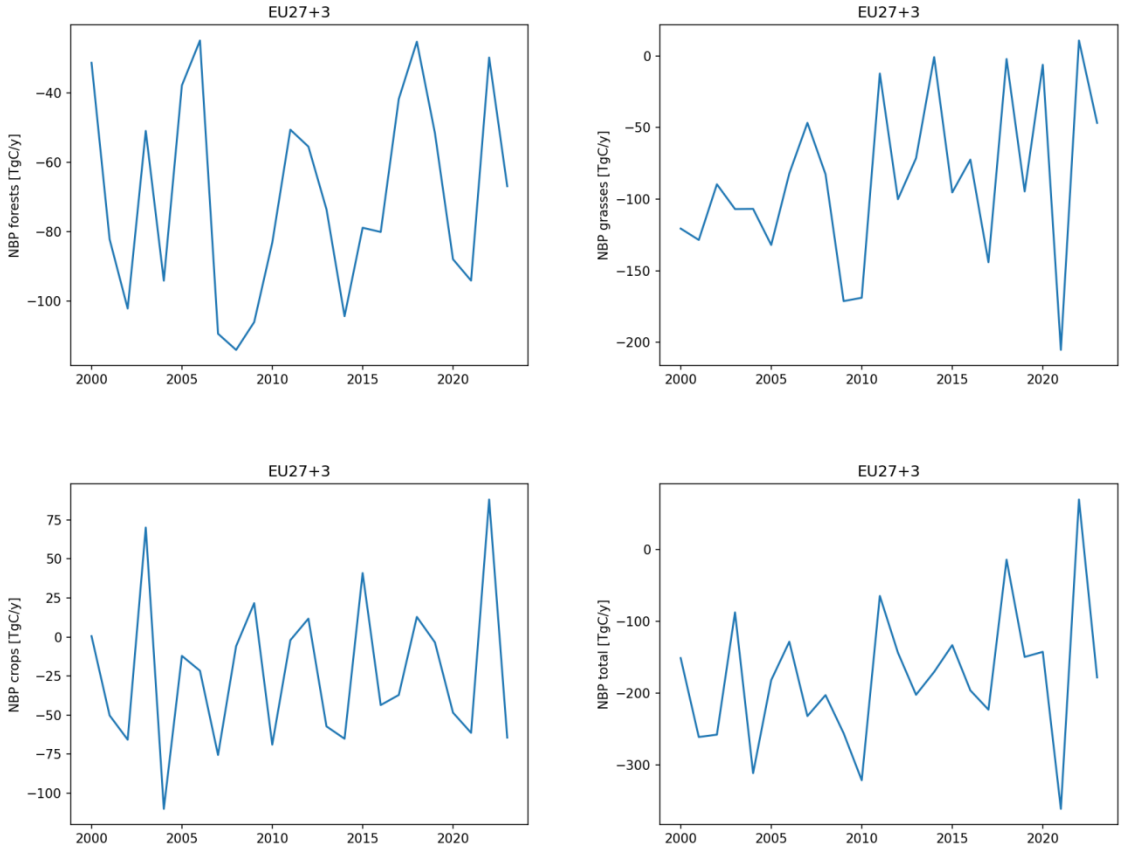

Figure 2.1.2: *Annual evolution of simulated net CO_2 fluxes (NBP) from ORCHIDEE over the EU27+3 (UK + Switzerland + Norway) for the forest (upper left), grassland (upper right) and cropland ecosystems (lower left), as well as for the total flux (lower right). Negative values indicate an ecosystem uptake of C.*

2.2 LPJ-GUESS

Overall model description

LPJ-GUESS is a process-based global vegetation model that can be used to investigate plant and soil C-N dynamics and their interactions in response to changes in environment (e.g., climate, atmospheric CO_2 levels, and N deposition) and management (e.g., conservation agriculture, forest thinning and clear-cutting) through simulating individual- and patch-level plant physiological and biogeochemical processes on a daily time step (Smith et al., 2014). Within the EYECLIMA framework, natural vegetation in the model is characterized by 22 European plant functional types (PFTs), with 20 woody and two herbaceous types included. PFTs differ in their phenology, photosynthetic pathway (C3 or C4), growth strategy, and bioclimatic limitations. Pastures are described as the competition between C3 and C4 grass PFTs, with half of aboveground biomass harvested annually to represent grazing impacts (Lindeskog et al., 2013). At present, LPJ-GUESS cannot simulate pasture management with dynamically varying N fertilizer application across time and space. To reflect the widespread use of synthetic fertilizer on European agricultural soils, we therefore assume that pasture receives a constant N application rate of 20 kg N ha^{-1} yr^{-1} from 1990 onward, corresponding to the 1990-2023 European average reported by Tian et al. (2022). Managed forest in the model is parameterized by even-aged or uneven-aged silvicultural systems through a user-defined regime which initiates a naturally regenerated or planted forest stand at the patch level. It includes a comprehensive set of parameters regulating timing and extent of planting, thinning and clear-cutting for individual tree species (Lindeskog et al., 2021). To represent cropland production over Europe, six crop functional types (CFTs): two temperate C3 crops with spring and

This project has received funding from the European Union's Horizon Europe research and innovation programme under grant agreement No 101081395

autumn sowing dates, a tropical C3 crop representing rice, a C4 crop representing maize, and two N-fixing grain legumes representing soybean and pulses, are simulated, with crop-specific differences in morphological traits, dynamic C-N allocation patterns, heat requirements for growth, and N fertilization management (Olin et al., 2015; Ma et al., 2022). Due to the absence of crop-specific calendar information for high-resolution simulations over Europe, the sowing date in each grid cell depends on a set of rules driven by crop- and climate-specific characteristics, with five seasonality types represented (see Waha et al. (2012) for details).

Model protocols for EYE-CLIMA simulations

Model spin-up follows the protocol in Ma et al. (2022). All simulations are initialized with a 1000-year spin-up using atmospheric carbon dioxide (CO_2) concentration from 1901 and repeating de-trended climate from 1901-1930. During spin-up, potential natural vegetation is simulated for the first 970 years, and then the cropland fraction linearly increases from zero to the first historic value (1901) in the last 30 years. Monthly atmospheric N deposition simulated by CCMI (NCAR Chemistry-Climate Model Initiative) from 1901 to 2023 is used and interpolated to the same resolution of the climate forcing (0.125°×0.125°; see below for details) (Tian et al., 2018).

Model experiments start with the year 1901 and run throughout the historical period until 2023 after model spin-up.The standard cropland managements (i.e., conventional tillage, 25% of residue retention, N fertilizer and manure application, and no cover crops), fertilized pasture (since 1990), managed forest (i.e., clear-cutting and Reineke self-thinning harvest), and unmanaged natural vegetation are simulated. For regional-scale application, LPJ-GUESS is driven by daily mean air temperature, precipitation, solar radiation, relative humidity, and wind speed from the observation-based CRU-ERA5 data set, spanning from 1901-2023 at 0.125° resolution. Annual atmospheric CO_2 concentration is from Meinshausen et al. (2020). Historical land use/land cover input data between 1901 and 2020 are adopted from HILDA+ (Winkler et al., 2021) and are aggregated from 0.01° to 0.125° with fractions of natural vegetation, managed forest, pasture, and cropland given for each grid cell. The European forest age data set in 2010 from Pucher et al. (2022) is used to initialize the timing of clear-cutting across all tree species in managed forest. In order to obtain forest age between 100-140 years descried in Pucher et al. (2022), the land use/land cover data from HILDA+ is further extended back to 1870. The growth distribution of various crop types, distinguishing shares of rain-fed and irrigated crop-specific fraction per grid cell, is based on the MIRCA data set around the year 2000 (Portmann et al., 2010) and aggregated to the six CFTs simulated over Europe. In terms of N fertilization, CFT-specific industrial N fertilizer and manure inputs are derived from HaNi data set (Tian et al., 2022), ranging from 1901-2019 at 0.125° resolution. Since regional-scale statistics on the timing of N fertilization in crops do not exist, in LPJ-GUESS we assume that synthetic N fertilizer is added to the soil mineral N pool for plant uptake at three crop development stages, with varying application rates for each CFT (Olin et al., 2015). Manure is applied as a single input to cropland at sowing to account for the time required for manure N to be made available for crops. As soil input, a soil map with fractions of clay, silt, and sand from the WISE30sec data set (Batjes, 2016) is used to parameterize soil hydraulic properties. For the second-round deliverable within the EYE-CLIMA framework, the three CO_2 flux components: gross primary productivity (GPP), heterotrophic respiration (Rh), and net biome productivity (NBP), together with soil N_2O emissions across natural, forest, pasture, and crop ecosystems are computed and provided over Europe with a daily time step.

Main results for CO_2 fluxes

European CO_2 fluxes from the terrestrial ecosystems simulated by LPJ-GUESS are shown as a map in Fig. 2.2.1 and as a time series between 1990-2023 in Fig. 2.2.2, with the annual total NBP over the recent two decades given in Table 2.2.1. Low GPP values across all ecosystems are found in the eastern and northern parts of Europe (such as Ukraine, Sweden, and Norway), with simulated values ranging

This project has received funding from the European Union's Horizon Europe research and innovation programme under grant agreement No 101081395

from 0 - 0.3 kgC m^{-2} yr^{-1}. In contrast, modelled GPP over Ireland, northern Spain, and the Balkan countries is as high as 1.2 - 1.5 kgC m^{-2} yr^{-1}. NBP, representing the net balance of CO_2 input and output in biosphere, shows a more complex spatial pattern between 2014-2023: the biogenic flux present a stronger sink of CO_2 in some boreal and temperate forests (-0.2 to -0.1 kgC m^{-2} yr^{-1} of NBP), in comparison with the NBP range of 0.15 to 0.2 kgC m^{-2} yr^{-1} in northern Germany, eastern England, and northwest France. In these regions, substantial carbon is removed from ecosystems annually through cropland harvest, resulting in a significant C source (Fig. 2.2.1).

Year-to-year of the CO_2 fluxes shows an increasing (GPP and Rh) or decreasing (NBP) trend over the simulation period, but with large variability between individual years (Fig. 2.2.2). Natural vegetation and managed forests are simulated as the two largest CO_2 sinks in European terrestrial ecosystems between 2000-2023, while croplands act as strong C sources due to their high harvest C fluxes. The simulated NBP in 2023 for these three vegetation types are –95.7, -86.8, and 22.8 TgC yr^{-1}, respectively. The aggregated C flux across all ecosystems shows a weak source or neutral CO_2 in the typical drought years (e.g., 57.4 and –5.9 TgC for the year 2003 and 2022, respectively), compared with the net C sink of -49.7 TgC yr^{-1} averaged the period of 2000-2023 (Table 2.2.1).

Table 2.2.1: *Total net biome production (NBP; TgC yr^{-1}) simulated by LPJ-GUESS in natural vegetation, pasture, managed forest, and cropland for EU27+3 countries between 2000-2023. Negative values indicate C sink.*

Year	Natural TgC yr^{-1}	Pasture TgC yr^{-1}	Managed forest TgC yr^{-1}	Cropland TgC yr^{-1}	Total TgC yr^{-1}
2000	-11.2	-22.4	-101.5	64.4	-70.7
2001	-29.4	-42.4	-95.7	24.7	-142.7
2002	-94.8	-36.3	-164.7	71.8	-223.9
2003	-30.4	54.9	-66.8	99.7	57.4
2004	-89.4	-61.0	-164.0	0.83	-313.6
2005	-42.0	2.8	-62.0	69.6	-31.6
2006	-35.4	39.4	-72.9	96.2	27.3
2007	-72.6	-101.4	-133.9	25.9	-281.9
2008	-92.4	-16.4	-149.9	26.1	-232.5
2009	-62.5	3.8	-103.8	41.1	-121.3
2010	-97.4	-21.0	-136.8	17.1	-238.1
2011	-79.0	-0.2	-98.9	58.8	-119.2
2012	-66.9	-22.7	-76.7	22.0	-144.3
2013	-71.4	40.8	-107.4	32.4	-105.6
2014	-107.4	-69.7	-154.2	34.9	-296.4
2015	-74.7	51.4	-100.2	50.9	-72.6
2016	-80.9	-59.8	-109.8	11.8	-238.8
2017	-46.9	5.3	-87.8	40.6	-88.8
2018	-90.4	42.4	-147.2	74.0	-121.2
2019	-127.8	-32.6	-170.8	8.4	-322.8
2020	-103.1	-3.7	-146.6	-1.4	-254.7

This project has received funding from the European Union's Horizon Europe research and innovation programme under grant agreement No 101081395

2021	-139.8	-50.7	-158.7	-11.6	-360.8
2022	-79.4	90.5	-86.3	69.2	-5.9
2023	-95.7	-9.2	-86.8	22.8	-168.9

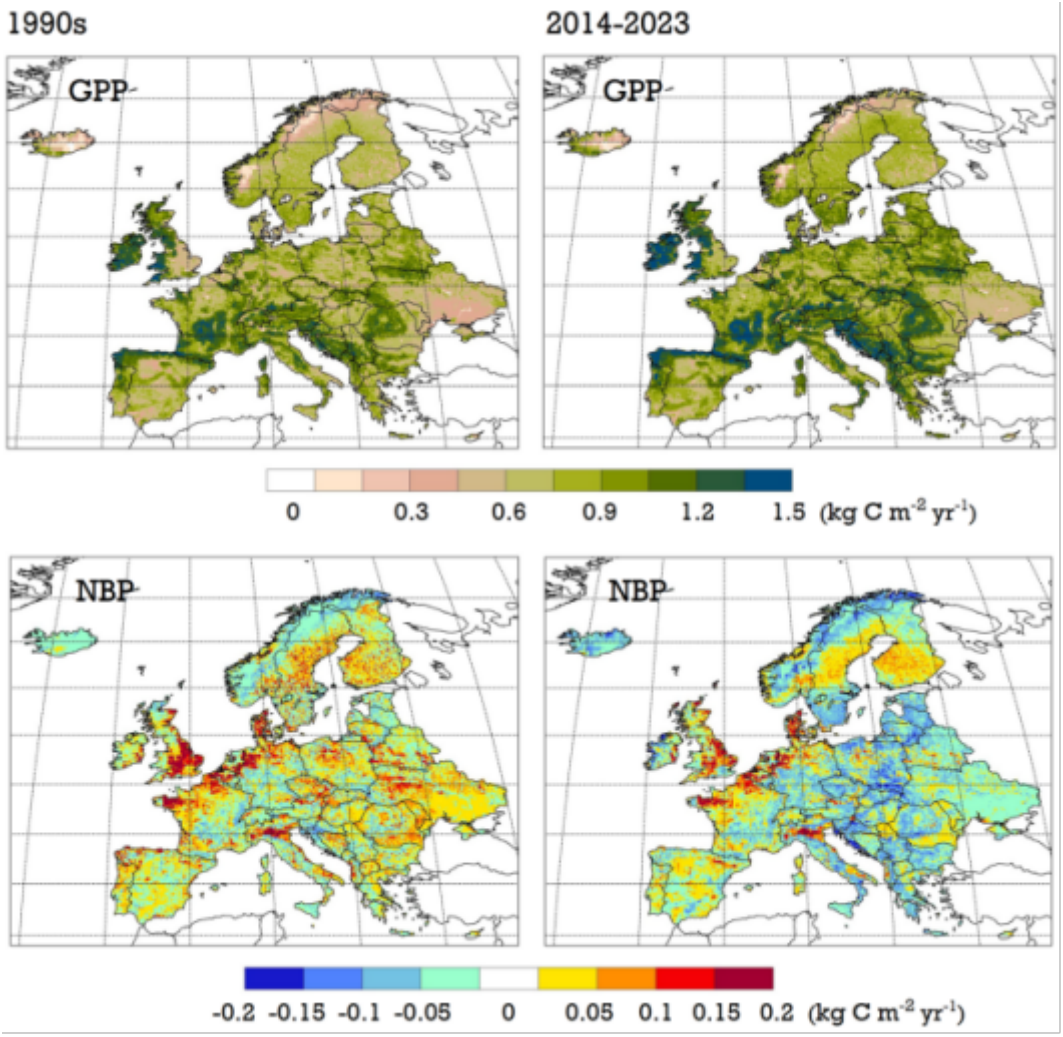

Figure 2.2.1: *Maps of simulated CO_2 fluxes across all land ecosystems by LPJ-GUESS, representing aggregated results from natural vegetation, pasture, managed forest, and cropland. GPP with positive flux indicates a C uptake.*

This project has received funding from the European Union's Horizon Europe research and innovation programme under grant agreement No 101081395

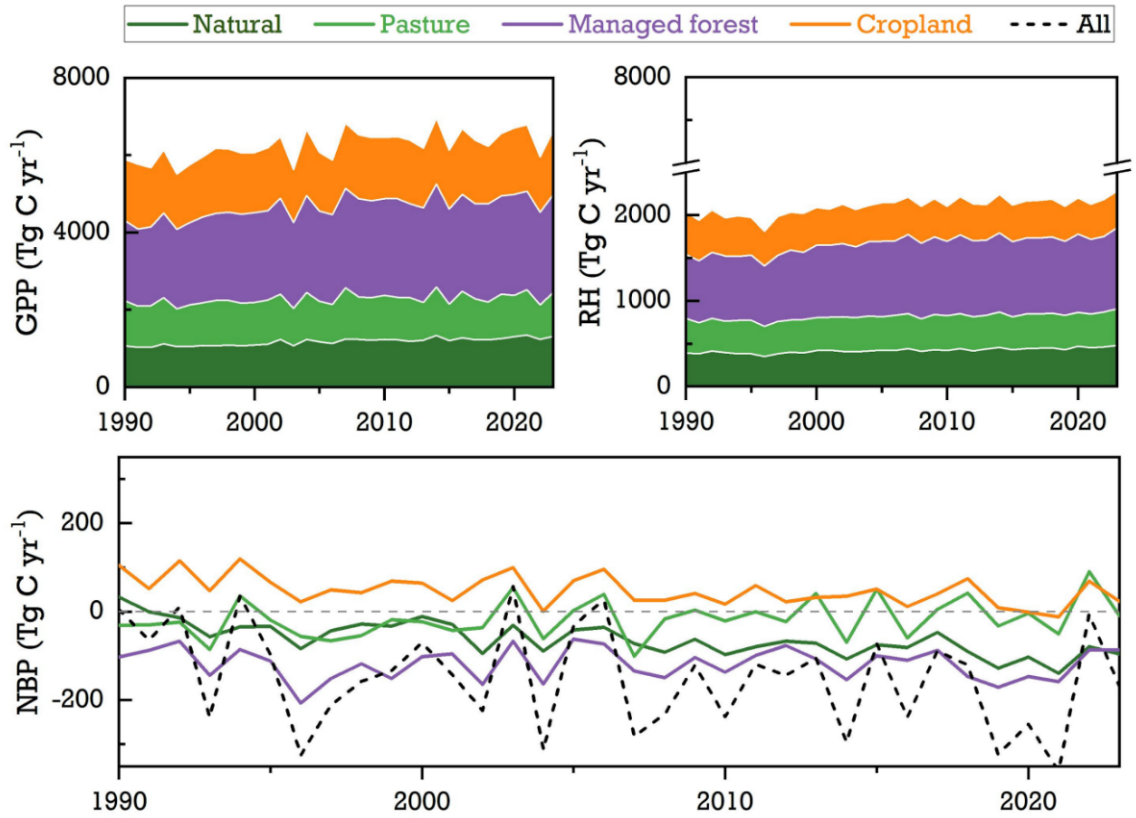

Figure 2.2.2: *Simulated total annual CO_2 fluxes (Tg C yr^{-1}) in natural vegetation, pasture, managed forest, and cropland by LPJ-GUESS over EU27+3 countries between 1990-2023. Negative values of NBP indicate a sink.*

2.3 Comparison between ORCHIDEE and LPJ-GUESS CO_2 fluxes

Comparison of the GPP fluxes

We first compare the spatial distribution of the GPP between the two models. Figure 2.3.1 displays the difference between ORCHIDEE and LPJ-GUESS over the 2014 - 2023 period. ORCHIDEE tends to simulate higher GPP over the north-central part of Europe and the Scandinavian countries (differences up to 1 kg/m^2/yr), while LPJ-GUESS simulates higher GPP in the southern part of Europe with also differences up to 1 kg/m^2/yr. The larger GPP values in north central Europe in ORCHIDEE are likely due to the larger nitrogen input in the regions (fertilisation and deposition) combined with a high sensitivity of the model to nitrogen input (see next section).

This project has received funding from the European Union's Horizon Europe research and innovation programme under grant agreement No 101081395

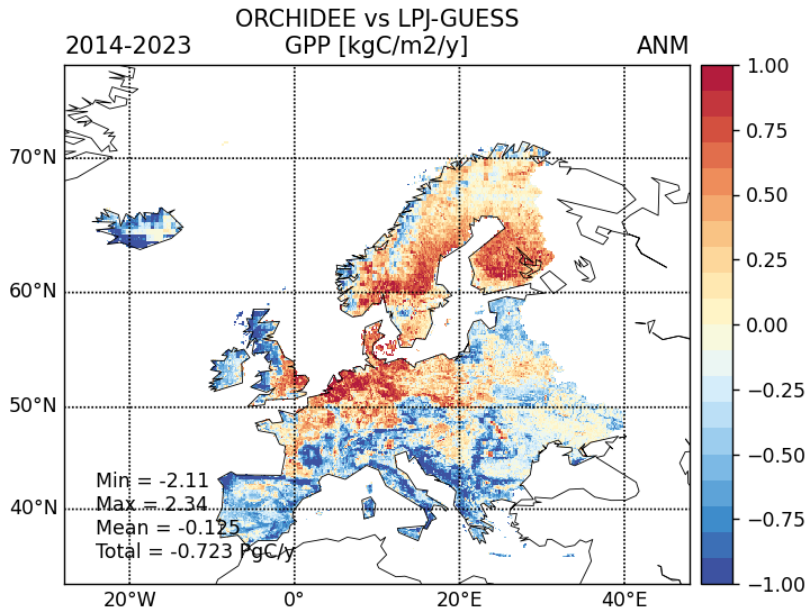

Figure 2.3.1: *Mean annual GPP differences between ORCHIDEE and LPJ-GUESS over the period 2014-2023. Positive values indicates a higher C uptake.*

We compared the ORCHIDEE and LPJ-GUESS GPP simulations with two independent estimates from a data-driven approach combining satellite observations and in-situ flux measurements:

- FLUXCOM-X-base product (Nelson et al., 2024; https://meta.icos-cp.eu/collections/AYj7-lwcdCLnBXJDoscxQZou)
- FluxSat v2.0 product (Joiner et al., 2018; https://avdc.gsfc.nasa.gov)

Both products were regridded to 0.1° resolution to match the model simulations. Figure 2.3.2 shows the temporal evolution over the period 1990 - 2023 of the annual GPP from the two models and the two data-driven products. We clearly see a strong correlation between the simulated fluxes by ORCHIDEE or LPJ-GUESS with the data-driven estimates for the total European domain as well as for the EU27+3 (EU27 plus UK, Switzerland and Norway), with R^2 values above 0.8. With respect to the mean values, both models are within the range provided by the two data-driven products with around 5.5 PgC/yr for the EU27+3. The overall trend of the GPP is positive (i.e., more carbon uptake) and coherent between all products with an increase of GPP around 0.5 PgC per decade over the period 1990 - 2020. For the global EU, the ORCHIDEE model is very similar with the FLUXCOM-X-Base product, while LPJ-GUESS is more in line with the FluxSat product. No specific reasons could be found in the structure of the model that could explain that one model is closer to a given benchmark.

Figure 2.3.2 provides similar comparisons but for a few individual countries (France, Germany, UK). At the country level we see larger differences between the different products. For France, while LPJ-GUESS is similar to FLUXCOM-X-Base, ORCHIDEE provides slightly lower GPP fluxes. This is the reverse for Germany with higher estimates from ORCHIDEE compared to the other products. For Hungary the two models provide very similar estimates in agreement with FLUXCOM-X-Base. More diagnostics comparing only the two models can be seen on a dedicated page: https://orchidas.lsce.ipsl.fr/dev/divers/eye-clima6.php.

This project has received funding from the European Union's Horizon Europe research and innovation programme under grant agreement No 101081395

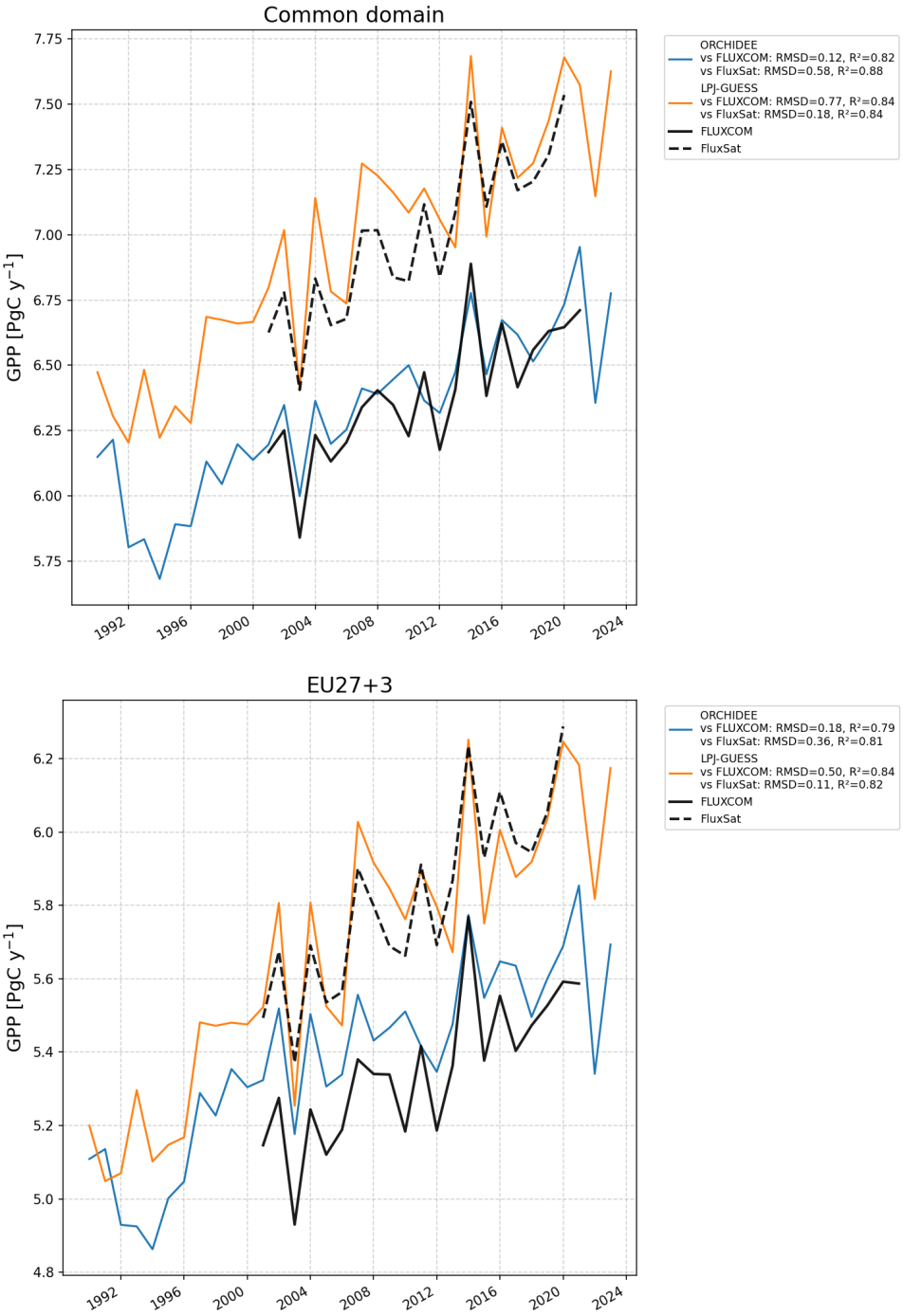

Figure 2.3.2: *Annual GPP estimates from ORCHIDEE and LPJ-GUESS models together with data-driven estimates from FLUXCOM-X-Base and FluxSat products, for two regions: top) European geographical domain (common to both model simulations) and bottom) the EU 27 plus UK, Switzerland and Norway. The correlation between each model and the two data products is provided in the legend.*

This project has received funding from the European Union's Horizon Europe research and innovation programme under grant agreement No 101081395

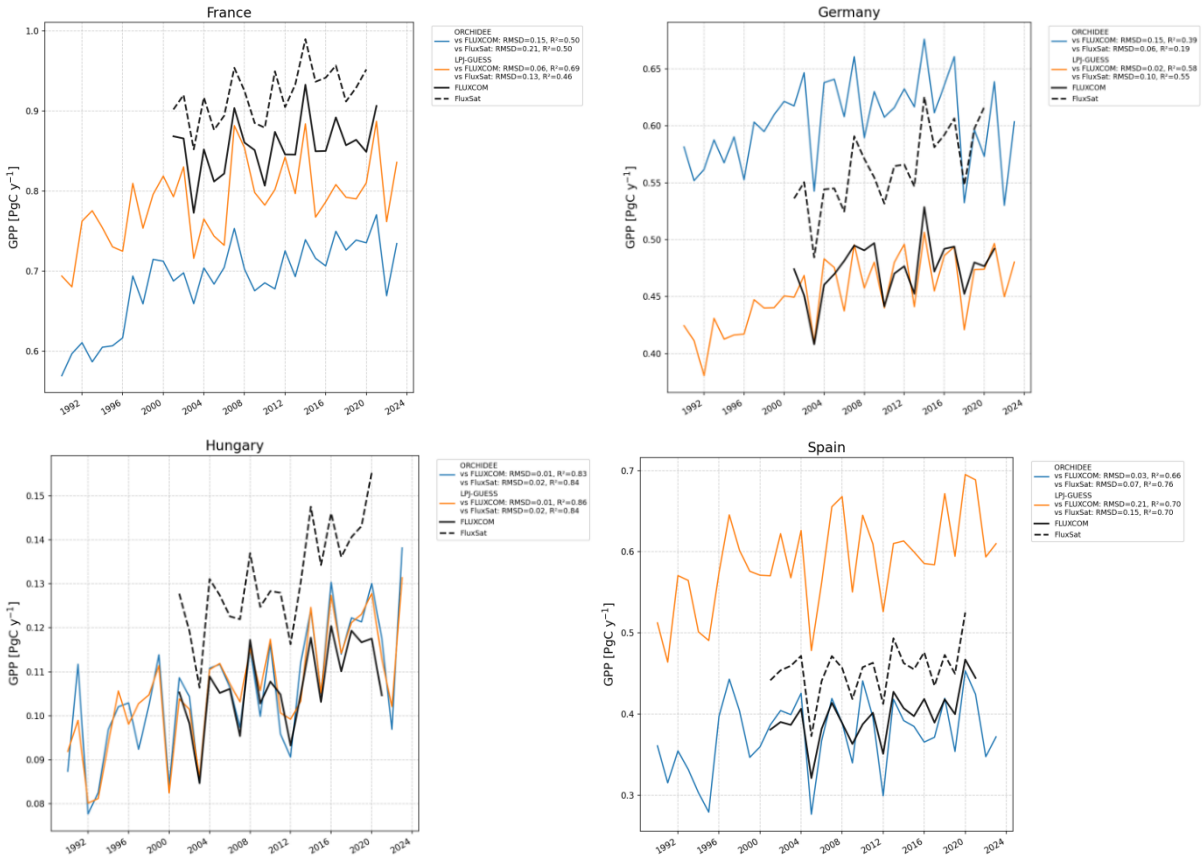

Figure 2.3.3: *Similar to figure 2.3.2 but for four different countries: France, Germany, Hungary and Spain.*

Comparison of the NBP fluxes

We now compare the ORCHIDEE and LPJ-GUESS net carbon fluxes, spatially and then aggregated for different European countries. Figure 2.3.4 displays the spatial mean NBP of the two models over the 2014 - 2023 period as well as the differences between ORCHIDEE and LPJ-GUESS. We clearly see that the two models provide different spatial patterns, with more fine scale structure in LPJ-GUESS compared to ORCHIDEE and on average a larger carbon uptake in the eastern part of Europe in LPJ-GUESS. If we focus on model differences, the spatial pattern of these differences shows a few similarities with the spatial pattern of GPP differences; for example, larger GPP are associated with larger NBP in ORCHIDEE over north Germany, Finland, eastern UK (see Figures 2.3.1 and 2.3.4). However, the NBP differences are smoother than the GPP differences due to other contributing fluxes that are in part proportional to the GPP (i.e., Respiration). Over the whole European domain, the mean carbon uptakes by the two models are relatively close, around 0.2 PgC/yr (see Figure 2.3.5 and Tables 2.1.1 and 2.2.1), with large year-to-year variations that are well correlated between the two models. For specific years, the amplitude of the anomalies (compared to the mean flux) significantly differs between the two models. For instance, the large drop in ecosystem carbon uptake in 2022 is more pronounced in ORCHIDEE, leading to a positive flux to the atmosphere, while for 1994 this is reverse with LPJ-GUESS having a small carbon flux to the atmosphere. In 2003, LPJ-GUESS also showed a strong negative anomaly with carbon release in the atmosphere while ORCHIDEE simulates only a small anomaly with still a large carbon uptake.

At the country level, the differences between the two models are slightly more pronounced, although the correlation between the annual flux variations are still large (Figure 2.3.5). For France, the year-to-year variability is larger in LPJ-GUESS: only the year 2022 is a source of carbon to the atmosphere for ORCHIDEE while for LPJ-GUESS the years 1990, 1994, 2003, 2006, 2015 and 2022 are a source. For Germany, reversely ORCHIDEE has a slightly larger year-to-year variability, with a source of 40 TgC/yr

This project has received funding from the European Union's Horizon Europe research and innovation programme under grant agreement No 101081395

in 2018 and a sink of 60 TgC/yr in 2021, while LPJ-GUESS has much small flux changes for these two years. For Hungary, LPJ-GUESS simulates a sink around 10 TgC/yr, while ORCHIDEE is close to neutrality. For Spain, the two models agree very well, with a small net carbon sink but large year-to-year variability (around ±40 TgC/yr). More diagnostics can be found in the dedicated page: https://orchidas.lsce.ipsl.fr/dev/divers/eye-clima6.php

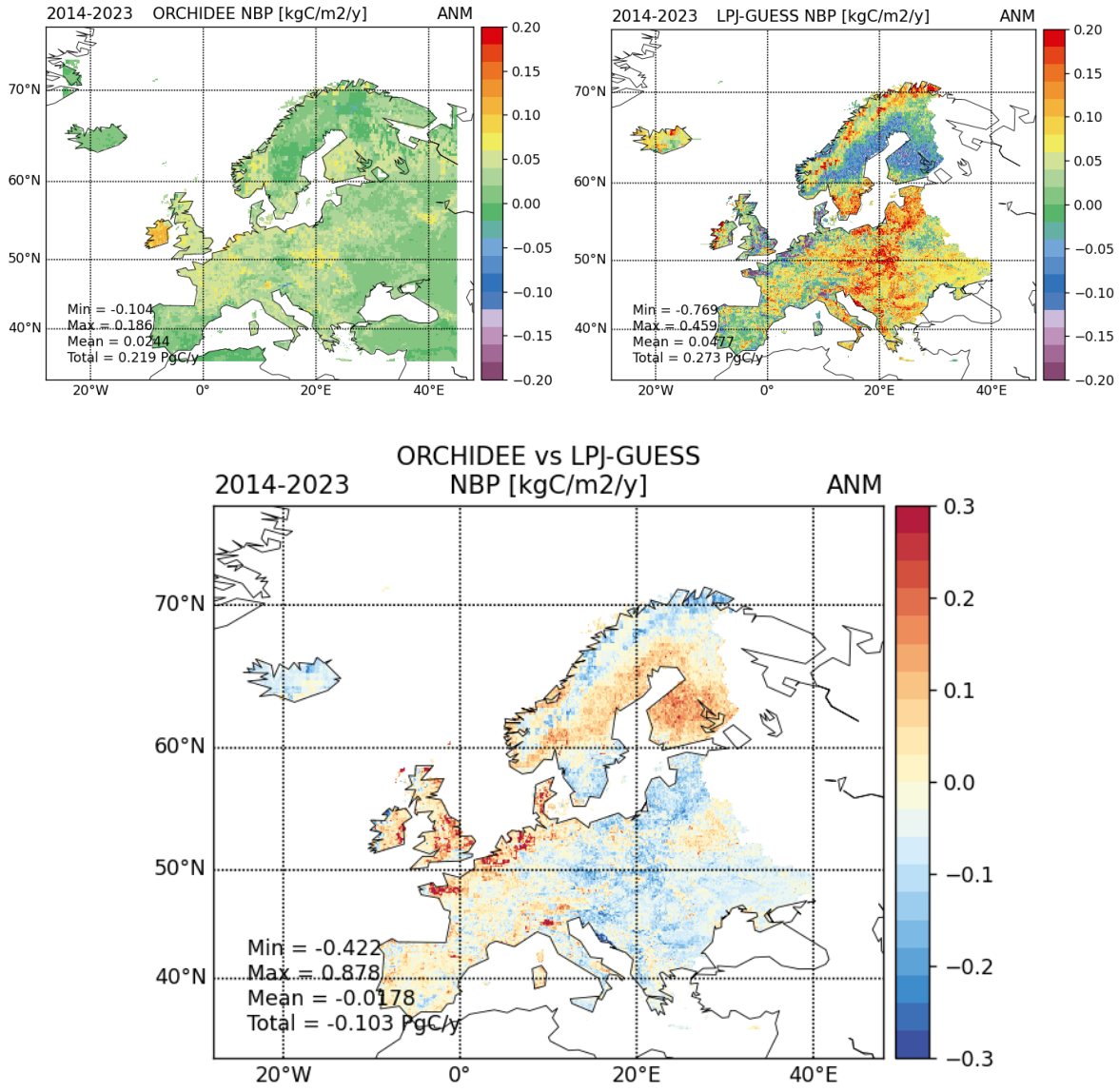

Figure 2.3.4: *Mean annual NBP for the two models ORCHIDEE and LPJ-GUESS and their differences (below plot) over the period 2014-2023. Positive NBP indicates a carbon uptake. For the map of the model difference, positive values indicate a larger carbon uptake for ORCHIDEE.*

This project has received funding from the European Union's Horizon Europe research and innovation programme under grant agreement No 101081395

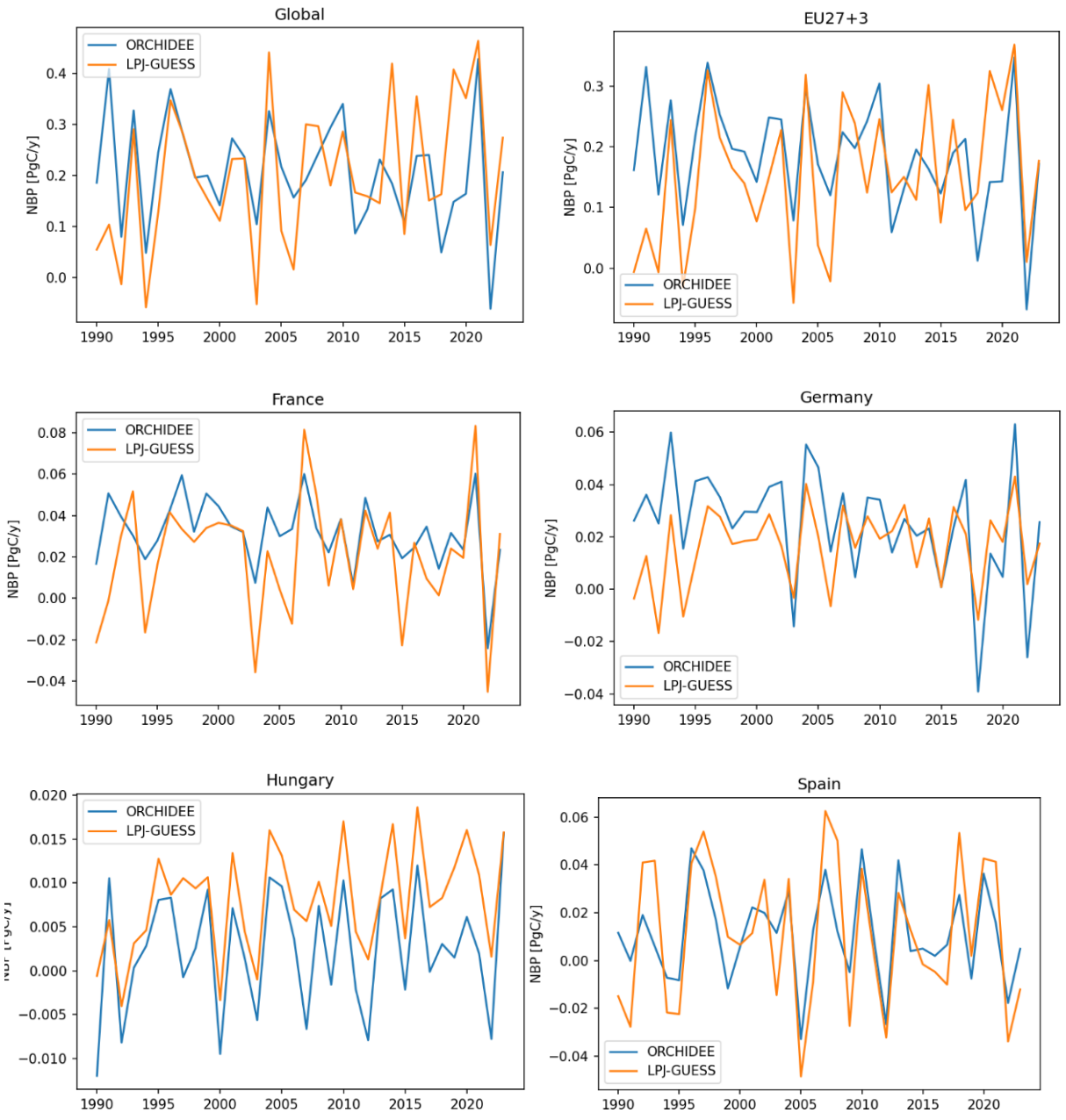

Figure 2.3.5: *Annual NBP estimates from ORCHIDEE and LPJ-GUESS models over the period 1990 - 2023 for several regions; top-left: European geographical domain (common to both model simulations); top-right: the EU 27 plus UK, Switzerland and Norway; middle-left: France; middle-right: Germany; bottom-left: Hungary; bottom-right: Spain. A positive flux indicates a carbon uptake by the vegetation.*

This project has received funding from the European Union's Horizon Europe research and innovation programme under grant agreement No 101081395

3. Process modelling of agricultural and forest land N_2O fluxes for Europe

3.1 ORCHIDEE

N cycle model description

The main features of the ORCHIDEE model are described in the section above for the CO_2 fluxes (section 2.1). Here, we thus only briefly describe the C-N dynamics that lead to the emissions of N_2O fluxes. Modelling of the mineral N dynamics by the ORCHIDEE model originates from the formulations used in the O-CN (Zaehle and Friend, 2010). It is composed of five pools for ammonium/ammoniac, nitrate, NOx, nitrous oxide, and dinitrogen forms. N_2O production in both nitrification and denitrification processes are represented. To be able to simulate co-occurring nitrification and denitrification processes in aerobic and anaerobic microsites, the soil is differentiated into aerobic and anaerobic fractions based on an empirical relationship linking oxygen consumption due to soil respiration (both below ground autotrophic and heterotrophic) and oxygen diffusion into the soil, which is itself functions of soil moisture (Li et al., 2000) and soil temperature. The potential daily rate of nitrification (R_{nit}) occurs only on the aerobic fraction of the soil and is a function of temperature, pH, and ammonium concentration (C_{NH4}):

$$R_{nit} = (1 - f(WFPS))\, f(T1)\, f(pH1)\, k_{nit}\, C_{NH4}$$

where k_{nit} is the reference potential NO_3^- production per mass unit of ammonium.

Mineral nitrogen inputs in the soil-plant system are related to:

- Atmospheric nitrogen deposition in the form of NH_x and NO_y components
- Biological nitrogen fixation (BNF) on any land category. The BNF rates are calculated as a function of evapotranspiration using the (Cleveland et al., 1999) method. In particular, all simulations employ a single evapotranspiration climatology based on a worldwide ORCHIDEE simulation for present-day conditions
- Nitrogen fertilization on croplands as well as on grassland. Note that ORCHIDEE does not separate pasture from rangeland, the nitrogen fertilization for pasture is applied to all grassland.

These input data were taken from the TRENDY intercomparison project (Sitch et al., 2024) which follow closely those derived within the NMIP model intercomparison project (Tian et al., 2018).

ORCHIDEE N_2O fluxes

Figure 3.1.1 displays the spatial distribution of the total N_2O fluxes across Europe as simulated by ORCHIDEE for the last decade (2014-2023), while Figure 3.1.2 reveals the temporal evolution for the EU27+3 (UK, Switzerland, Norway) of the total flux and the contributions from grassland, cropland and forests, for the period 2000 - 2023. Table 3.1.1 also provides the values of these grassland, cropland and forest fluxes for the EU27+3. The mean flux across geographical Europe is around 0.122 gN/m^2/yr, with a large peak around the most industrialised region of Europe (i.e., the Netherlands with fluxes around 0.5 gN/m^2/yr) where the N deposition and N fertilisation are the largest. The total flux for the EU27+3 is around 0.65 TgN/yr while for geographical Europe (the whole domain of Figure 3.1.1) it is around 1.1 TgN/yr. The temporal evolution of the total N_2O flux shows moderate year-to-year variations, between 0.6 and 0.7 TgN/yr; the largest emission is simulated in 2011 (associated with low precipitation) and the lowest in 2012. Total forest fluxes are two times smaller than the cropland and grassland fluxes but the three flux components show significant year-to-year correlations. Both cropland and forest fluxes show a small decrease after 2010, due possibly to reduction of N deposition, while the grassland flux does not show a significant trend.

This project has received funding from the European Union's Horizon Europe research and innovation programme under grant agreement No 101081395

Note that the simulated fluxes by ORCHIDEE have slightly changed compared to the previous version of this deliverable. The main reason was due to changes in the nitrogen input dataset that was revised, as it was initially leading to spurious grassland flux increase in 2020-2022 that is no longer present.

Additional plots are also available under a dedicated website: https://orchidas.lsce.ipsl.fr/dev/divers/eye-clima6.php.

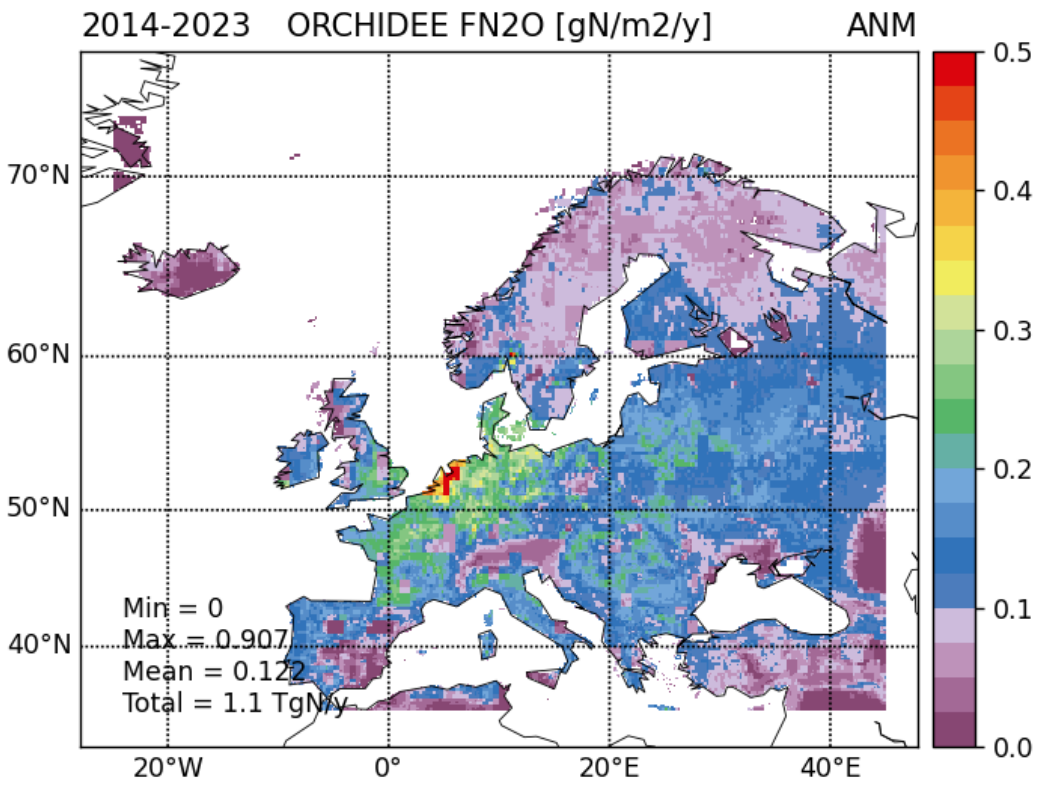

Figure 3.1.1: *Maps of simulated N_2O emissions for all ecosystems by ORCHIDEE over EU27+3 countries, averaged over 2012 and 2022.*

This project has received funding from the European Union's Horizon Europe research and innovation programme under grant agreement No 101081395

Table 3.1.1: *Total soil N_2O emissions (TgN yr^{-1}) simulated by ORCHIDEE in forest vegetation, grassland, and cropland for EU27+3 countries between 2000-2022.*

Year	Forest TgN yr^{-1}	Grassland TgN yr^{-1}	Cropland TgN yr^{-1}	Total TgN yr^{-1}
2000	0.149	0.26	0.233	0.642
2001	0.153	0.254	0.233	0.64
2002	0.151	0.254	0.225	0.63
2003	0.155	0.273	0.243	0.672
2004	0.155	0.268	0.243	0.666
2005	0.15	0.253	0.233	0.636
2006	0.158	0.255	0.238	0.651
2007	0.164	0.259	0.235	0.658
2008	0.148	0.234	0.22	0.602
2009	0.151	0.242	0.228	0.621
2010	0.162	0.234	0.238	0.635
2011	0.171	0.264	0.257	0.692
2012	0.136	0.233	0.216	0.585
2013	0.165	0.238	0.236	0.639
2014	0.161	0.254	0.244	0.658
2015	0.152	0.251	0.241	0.644
2016	0.145	0.24	0.22	0.605
2017	0.143	0.257	0.233	0.633
2018	0.156	0.259	0.235	0.651
2019	0.144	0.259	0.222	0.625
2020	0.152	0.267	0.222	0.642
2021	0.153	0.257	0.222	0.632
2022	0.141	0.26	0.215	0.616
2023	0.15	0.256	0.212	0.619

This project has received funding from the European Union's Horizon Europe research and innovation programme under grant agreement No 101081395

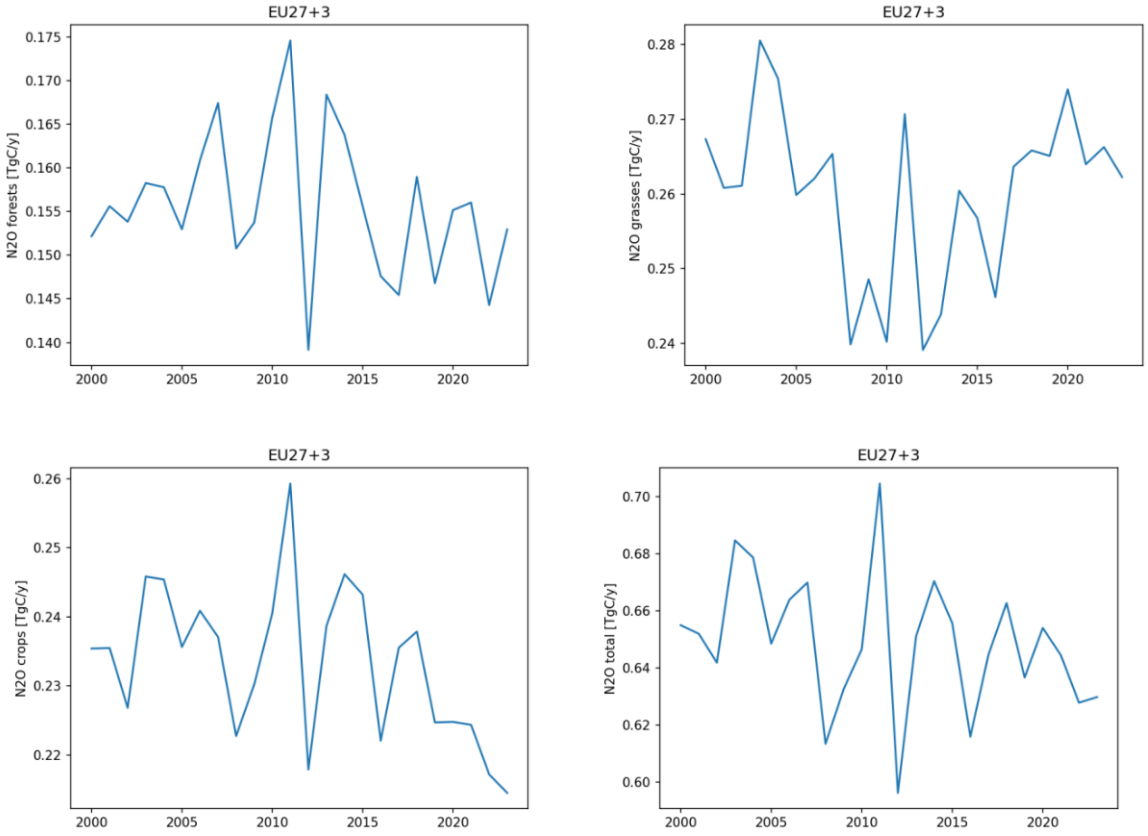

Figure 3.1.2: *Annual evolution of simulated N_2O emissions from ORCHIDEE over the EU27+3 (UK + Switzerland + Norway) for the forest (upper left), grassland (upper right) and cropland (lower left) ecosystems, as well as for the total flux (lower right).*

3.2 LPJ-GUESS

N cycle model description

Soil C-N dynamics in LPJ-GUESS are simulated by a soil organic matter (SOM) scheme derived from the Century model (Parton et al., 1993), in which SOM and litter are characterized by 11 pools with prescribed C:N ratios and decay rates (B. Smith et al., 2014). The transfer of SOM between pools drives N mineralization or immobilization, as a result of the altered C:N ratios in the donor and receiver pool. Net N mineralization (i.e., mineralization minus immobilization), together with industrial N fertilizer and atmospheric N deposition, determine the size of the total soil mineral N pool, which is depleted by plant N uptake, as well as by ecosystem N losses through N leaching and gaseous N emission on a daily time step (Zaehle & Friend, 2010; Wårlind et al., 2014). Gaseous N emission produced in the soil to the atmosphere is simulated as NH_3, NO_x, N_2O, and N_2, with the representation of soil N dynamic processes including NH_3 volatilization, nitrification, and denitrification in the SOM pools. Within the EYE-CLIMA framework, we have updated a detailed representation of soil N transformation scheme adopted from the DyN model (Xu-Ri & Prentice, 2008) and the CLM5 model (Val Martin et al., 2023).

Microbial processes in soils occur on short time-scales and spatially in a highly heterogeneous pattern. A number of factors influence the nitrification and denitrification rates where the processes are not fully understood, and where the influence of the major controlling factors is not easily defined; factors can have multiple roles and interact with other factors. Nonetheless, key N transformations of soil mineral N are reported to be controlled by soil characteristics such as drainage (aeration, texture, compaction), temperature, moisture, pH, organic matter, available N substrate (NH_4 and NO_3), and C:N ratios of soil

This project has received funding from the European Union's Horizon Europe research and innovation programme under grant agreement No 101081395

organic matter. Accordingly, we implemented these critical limitating factors to the nitrification and denitrification processes in the model, following the empirical relationships between N transformation and environmental control factors presented in field experiments and other modelling studies (e.g., Weier et al., 1993; Maag & Vinther, 1996; Rochester, 2003; Liu et al., 2010; Wagena et al., 2017; Blanc-Betes et al., 2021; Zhang et al., 2023). The transformed N gases accumulate in the soil and are ultimately diffused into the atmosphere, depending on the soil aeration status and temperature. More details of N_2O-related processes implemented in LPJ-GUESS are provided in Ma et al. (2024).

Main results for N_2O fluxes

European soil N_2O emissions from the land ecosystems simulated by LPJ-GUESS are shown as a map in Fig. 3.2.1 and as time series between 1990-2023 in Fig. 3.2.2. The largest N_2O emissions from all ecosystems are found in central and eastern Europe, where the simulated rates are as high as 5.0 kgN ha^{-1} yr^{-1}; in comparison, northern Europe with cold climates shows less N emissions of 0-0.5 kgN ha^{-1} yr^{-1}, probably due to the slow turnover of the SOM pools and extensive N management in the high latitudes. Chemical N fertilizer in the model plays an important role in regulating N_2O emissions in European cropland, with the greatest fluxes found the highly fertilized soils (e.g., France, Germany, and UK); while the regions with less N inputs, such as Baltic countries, generally present as a weaker N_2O source (Fig. 3.2.1).

Cropland is simulated as the main contributor (52%) to the N_2O total emissions in European terrestrial ecosystems in 2023, followed by pasture (24%), managed forest (19%), and natural vegetation (5%), with the estimated emissions of 0.29, 0.13, 0.11, and 0.03 TgN yr^{-1} for these four land-use types, respectively (Table 3.2.1). We also found that the modelled total N_2O from the European cropland has shown a declining trend since the 1990s (Fig. 3.2.2), mainly because of reduced N fertilizer use over this timeframe. Compared with the high N_2O emissions on cropland, natural ecosystems in our simulations generally act as weaker N_2O sources, consistent with findings from field experiments and other modelling studies.

Table 3.2.1: *Total soil N_2O emissions (TgN yr^{-1}) simulated by LPJ-GUESS in natural vegetation, pasture, managed forest, and cropland for EU27+3 countries between 2000-2023.*

Year	Natural TgN yr^{-1}	Pasture TgN yr^{-1}	Managed forest TgN yr^{-1}	Cropland TgN yr^{-1}	Total TgN yr^{-1}
2000	0.029	0.081	0.073	0.362	0.545
2001	0.032	0.106	0.081	0.335	0.553
2002	0.034	0.104	0.086	0.383	0.606
2003	0.028	0.074	0.075	0.281	0.458
2004	0.027	0.108	0.078	0.299	0.512
2005	0.028	0.085	0.085	0.307	0.505
2006	0.032	0.104	0.090	0.269	0.494
2007	0.037	0.128	0.101	0.387	0.653
2008	0.027	0.079	0.085	0.292	0.483
2009	0.026	0.071	0.084	0.293	0.473
2010	0.029	0.095	0.082	0.281	0.487
2011	0.030	0.078	0.085	0.316	0.509

This project has received funding from the European Union's Horizon Europe research and innovation programme under grant agreement No 101081395

2012	0.031	0.082	0.088	0.288	0.488
2013	0.029	0.086	0.087	0.268	0.471
2014	0.036	0.106	0.100	0.354	0.595
2015	0.031	0.079	0.095	0.267	0.472
2016	0.030	0.095	0.096	0.293	0.513
2017	0.032	0.077	0.093	0.319	0.521
2018	0.027	0.078	0.086	0.308	0.500
2019	0.025	0.088	0.087	0.279	0.478
2020	0.024	0.101	0.089	0.290	0.504
2021	0.025	0.098	0.092	0.286	0.501
2022	0.026	0.079	0.094	0.246	0.445
2023	0.031	0.130	0.105	0.285	0.550

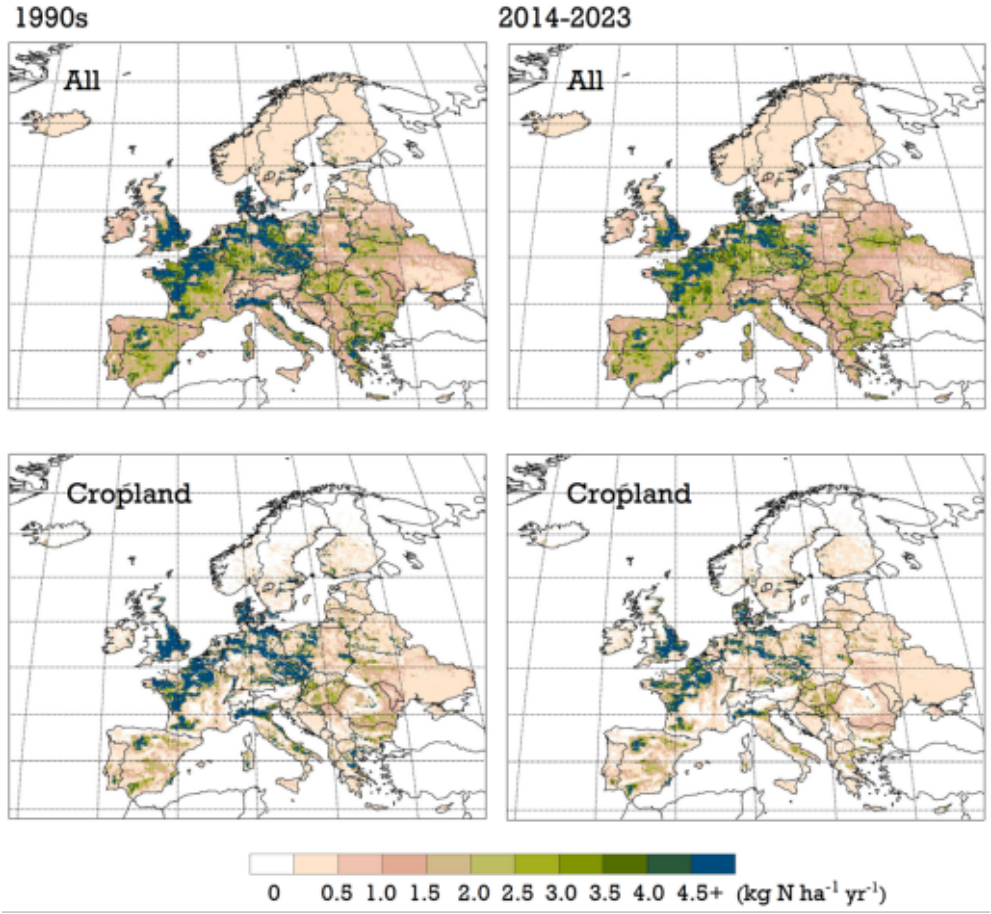

Figure 3.2.1: *Maps of simulated soil N_2O emissions by LPJ-GUESS in the 1990s and 2014-2023. 'All' represents aggregated results from natural vegetation, pasture, managed forest, and cropland.*

This project has received funding from the European Union's Horizon Europe research and innovation programme under grant agreement No 101081395

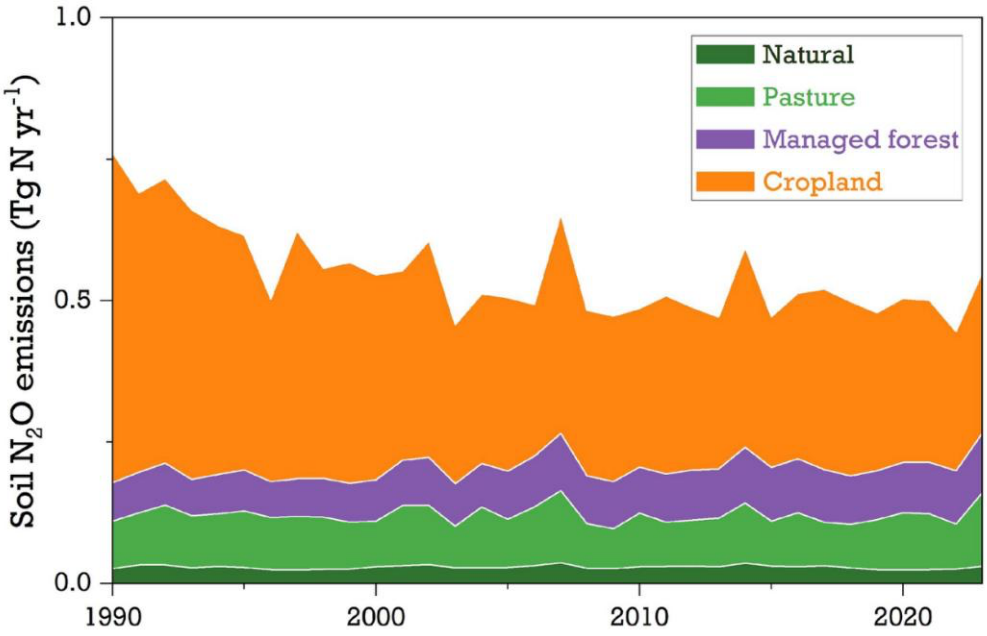

Figure 3.2.2: *Simulated total annual N_2O emissions (TgN yr^{-1}) in natural vegetation, pasture, managed forest, and cropland by LPJ-GUESS over EU27+3 countries between 1990-2023.*

3.3 Comparison between ORCHIDEE and LPJ-GUESS N_2O fluxes

As for CO_2, this section is a first step toward the quantification of the N_2O flux uncertainty with a comparison of the total emissions between the two models. Before comparing the simulated N_2O emissions, we first compared the nitrogen input used by both models, given that unfortunately these input data were not completely harmonized.

For the nitrogen deposition fluxes, we have used the same input fluxes for both models as illustrated in Figure 3.3.1. We clearly see a hot spot of N deposition over the northern central part of Europe (Netherlands and northern Germany) that is partly explaining the large N_2O emissions over these regions in both models but more specifically in ORCHIDEE.

For the nitrogen fertilisation rates (NH_4 and NO_3), both models use different input datasets, as illustrated in Figures 3.3.2 and 3.3.3. The mean difference between the two models shows that LPJ-GUESS uses higher emissions over Czech Republic and Turkey, while ORCHIDEE has slightly larger fertilisation rates over the central part of Europe and more specifically the Netherlands. The temporal evolution of the two fertilisation rates are relatively similar but the magnitude differs, more substantially for NH_4 than NO_3. For NH_4, fertilisation largely increased from the 1950s (with less than 2 TgN/yr for the European domain) to around 1990 (with more than 12 TgN/yr), with then a large drop during the early 90s followed (following environmental policies) by a slow increase. ORCHIDEE has the same temporal evolution but with larger fertilisation rates (around +2 TgN/yr). For NO_3, the temporal evolution of the two rates is similar, with LPJ-GUESS having slightly larger rates during the peak of fertilisation in the late 90s but then followed by a larger drop than ORCHIDEE with a minimum around 2010; the last decade is characterized by a slow increase, which is similar in the two models.

This project has received funding from the European Union's Horizon Europe research and innovation programme under grant agreement No 101081395

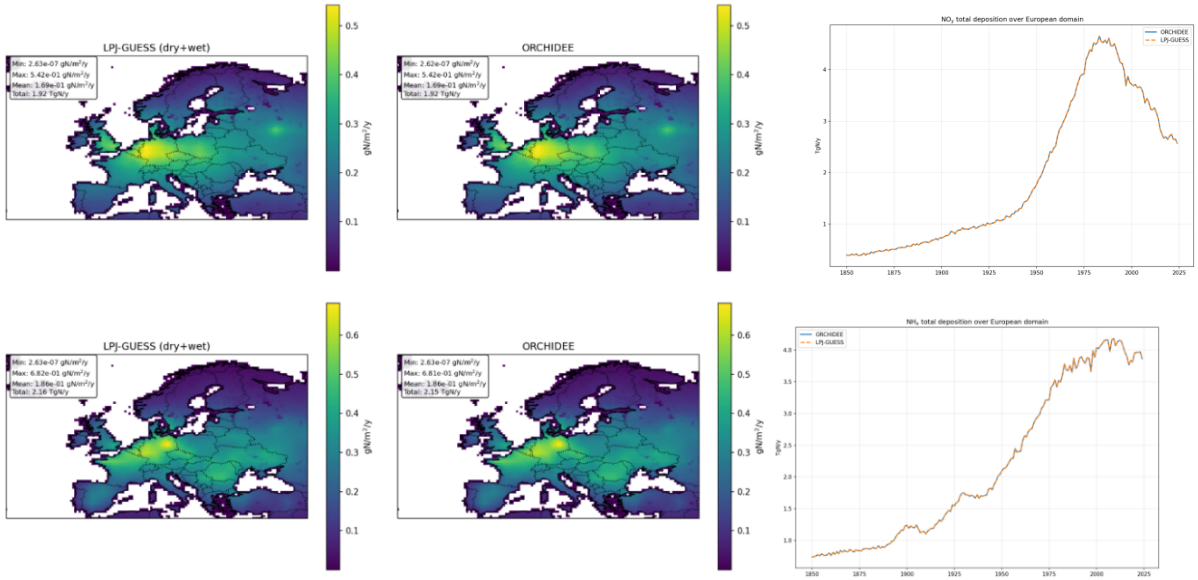

Figure 3.3.1: *Top: NOy deposition for the two models; left) maps of mean deposition over the period 1850-2024 in gN/m^2/yr and right) temporal evolution of the total deposition over Europe in TgN yr^{-1}. Bottom: Same but for NHx deposition. Note that ORCHIDEE and LPJ-GUESS time series overlap.*

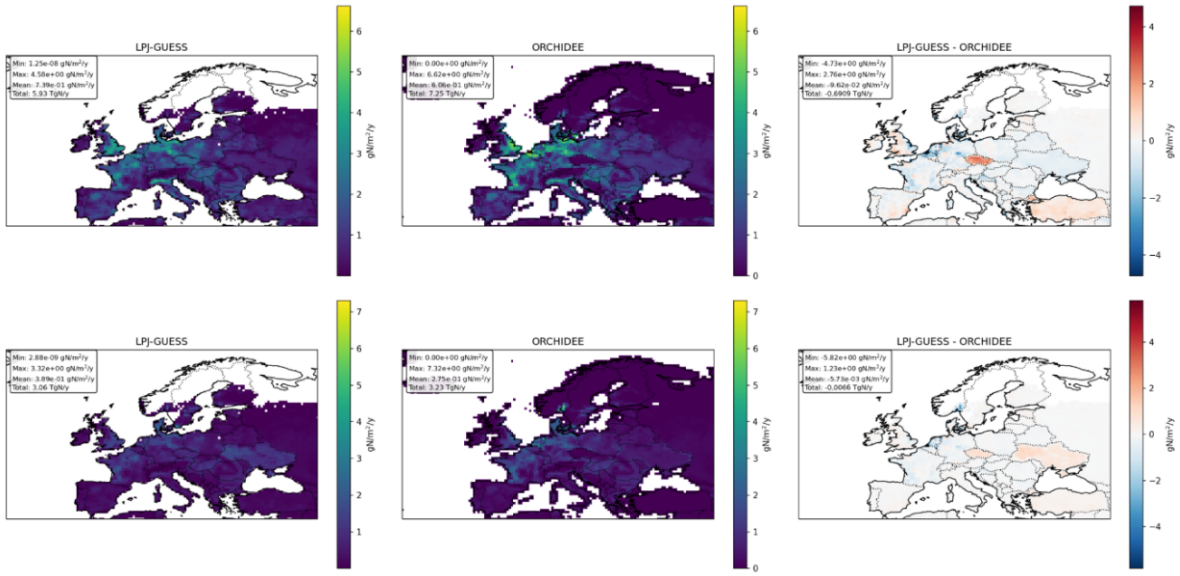

Figure 3.3.2: *Top) NH_4 fertilizer application for cropland used in LPJ-GUESS (left) and in ORCHIDEE (central) and the difference between the two models (right) in gN/m2/yr. Bottom) same diagnostic but for NO_3 fertilizer application for cropland. The data correspond to 1850-2024 averages.*

This project has received funding from the European Union's Horizon Europe research and innovation programme under grant agreement No 101081395

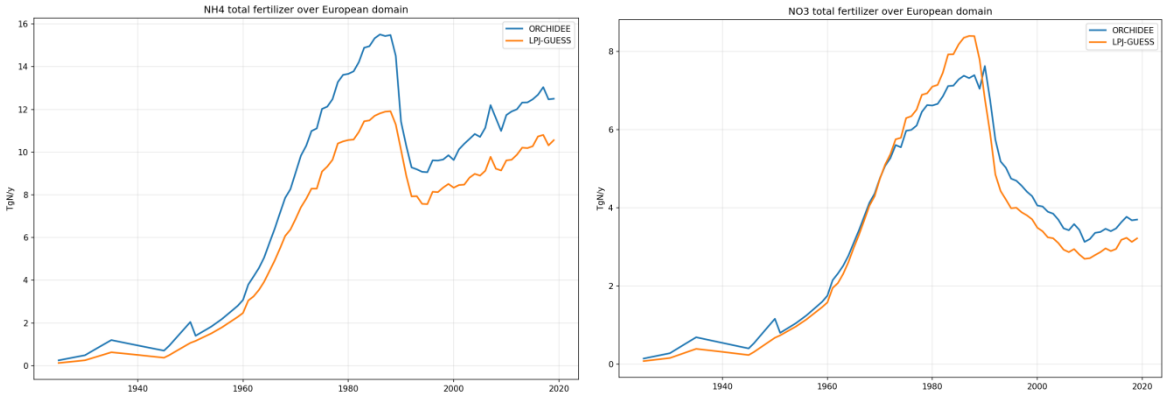

Figure 3.3.3: *Temporal evolution of the total NH_4 (left) and NO_3 (right) fertilizer applications for cropland for the two models LPJ-GUESS and ORCHIDEE. Note that both models do not use exactly the same cropland fraction.*

We now compare in Figures 3.3.4 and 3.3.5 the spatial distribution and the temporal evolution of the total N_2O emissions, respectively.

On average the two models produce similar total N_2O flux for Europe with, however, some differences in the spatial and temporal distributions. The hotspot of emission around the Netherlands in ORCHIDEE is less pronounced in LPJ-GUESS, while LPJ-GUESS has larger emissions in northern France, northern Germany and Poland associated with cropland and grassland. On average, ORCHIDEE has slightly larger N_2O fluxes in the northern countries, especially for the forest ecosystems. For the EU27+3 (UK, Switzerland, Norway) the mean flux of ORCHIDEE (around 0.65 TgN/yr, Figure 3.3.5) is slightly larger than LPJ-GUESS (close to 0.55 TgN/yr). For the EU27+3, the year-to-year variations of the fluxes are also different between the two models, LPJ-GUESS showing slightly larger variations than ORCHIDEE, with pronounced spikes in 2007 and 2014. In addition, LPJ-GUESS shows a decreasing trend in N_2O emissions for the EU27+3 between 1990 up to the end of the simulation in 2023; such a trend is not present in the ORCHIDEE model with relatively constant emissions over the three decades. The decreasing flux in LPJ-GUESS is associated with the cropland emissions (see Figure 3.2.2). It is the result of the large drop in nitrogen fertilisation that occurred in the early 1990s and that is impacting the N_2O emissions in the last two decades (2000s and 2010s) although the total nitrogen input was not decreasing anymore (i.e., a compensation between i) an increase of NH_4 fertilisation, ii) a slight decrease of NO_3 fertilisation up to 2010 and increase again, iii) decrease of NO_y deposition and iv) stable NH_x deposition). ORCHIDEE does not respond strongly to the big drop in fertilisation application in the early 90s with thus no legacy effects in the 2000s.

At country levels, there is no systematic difference between the two models for the mean flux and the interannual variations. For France and Germany, LPJ-GUESS has slightly larger emissions and larger year-to-year variability with also a decreasing trend not seen in ORCHIDEE. For Hungary and Spain, this is a bit the reverse with higher emission and larger year-to-year variations in ORCHIDEE; for these countries both models do not show a significant trend over the period 1990 - 2023. Overall, for each country, we do not see strong correlations between the year-to-year variations of the ORCHIDEE and LPJ-GUESS fluxes, which indicates that the factors controlling soil nitrogen dynamics in the two models are complex and do not simply follow meteorological drivers. Ongoing experiments are currently being carried out to analyse the drivers of these model differences.

This project has received funding from the European Union's Horizon Europe research and innovation programme under grant agreement No 101081395

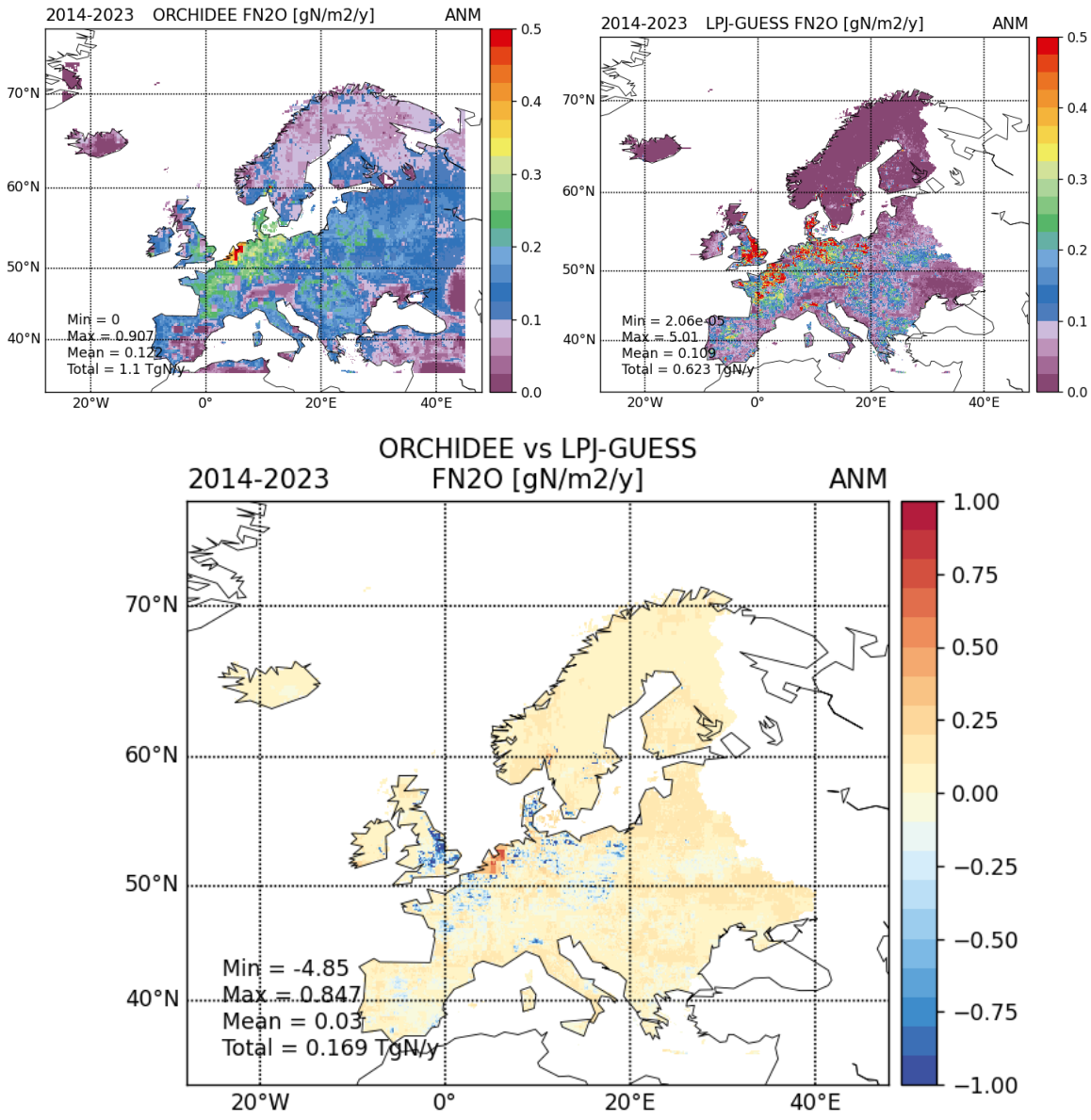

Figure 3.3.4: *Maps of simulated N_2O emissions from ORCHIDEE (top left) and LPJ-GUESS (top right) over Europe averaged over 2014 and 2023 with the difference map between the models (bottom).*

This project has received funding from the European Union's Horizon Europe research and innovation programme under grant agreement No 101081395

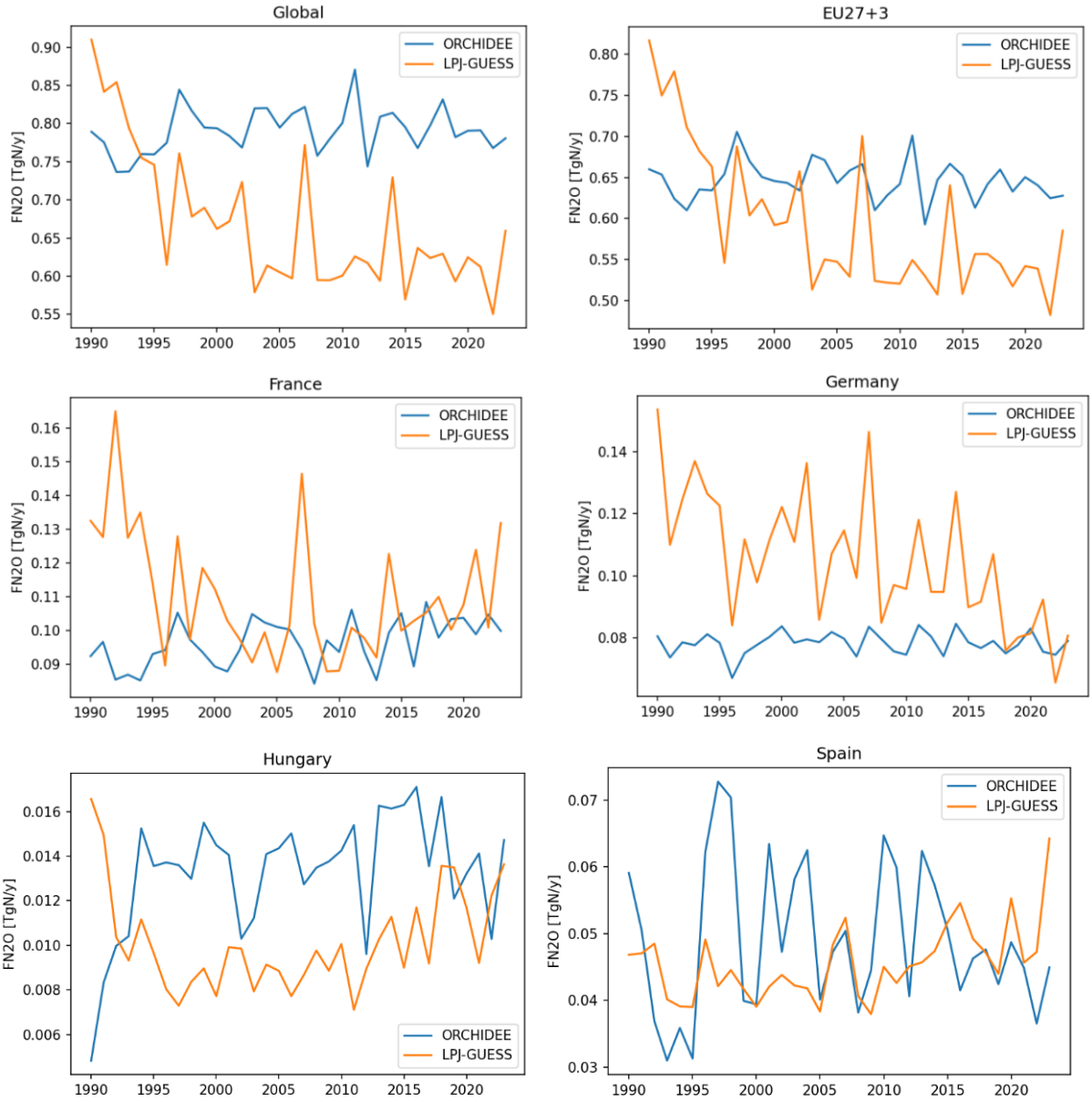

Figure 3.3.5: *Annual evolution of simulated N_2O emissions from ORCHIDEE and LPJ-GUESS models over the period 1990 - 2023 for several regions; top-left: European geographical domain (common to both model simulations); top-right: the EU 27 plus UK, Switzerland and Norway; middle-left: France; middle-right: Germany; bottom-left: Hungary; bottom-right: Spain.*

3.4 Investigation N_2O mitigation through management

Conservation agriculture, such as reduced tillage, residue retention, and legume cover crops, has for many years been recommended as a promising climate mitigation practice because of its ability to enhance soil carbon sequestration (Poeplau & Don, 2015; Smith et al., 2020). However, much experimental evidence showed that these conservation practices had a potential to offset the CO_2 mitigation effect due to the increased N_2O emissions (e.g., Lugato et al., 2018; Mei et al., 2018; Quemada et al., 2020; Yangjin et al., 2021). Given the limited adoption of conservation agriculture on current global croplands (Porwollik et al., 2019), LPJ-GUESS considers only conventional management in the simulation experiments in this project, with all European cropland grid cells adopting a uniform management intensity. This stylized model setup, with homogenous assumptions of management intensities, may introduce large uncertainties in N_2O estimates on croplands. For instance, the scenarios of model-based management simulations indicate that, compared with standard management (referred

This project has received funding from the European Union's Horizon Europe research and innovation programme under grant agreement No 101081395

to as STD in Table 3.4.1), implementing 100% crop residue retention (RR) and cover cropping systems may potentially enhance European cropland N_2O emissions in 2023 by 0.76 TgN (+205%) and 0.14 Tg N (+38%), respectively (Fig. 3.4.1). Likewise, adoption of legume cover crops (CC_L) poses a higher risk in increasing N_2O emissions than non-legume cover crops (CC_{NL}), primarily due to the unique ability of legumes to fix atmospheric nitrogen into the soil. In contrast, no-till management (NT) is identified as the only strategy to slightly mitigate N_2O emissions in the simulations, mainly as a result of the reduced net N mineralization rate following the introduction of conservation tillage systems.

The timing of N fertilizer application is another uncertain factor controlling N_2O emissions on croplands by affecting plant nitrogen use efficiency. In LPJ-GUESS we assume that synthetic N fertilizer is added to the soil mineral N pool for plant uptake at three crop development stages, with varying application rates for each crop type (i.e., STD in Table 3.4.1; Olin et al., 2015). Our model simulations of N fertilization management scenarios show that, compared with standard management (STD), applying all fertilizer at crop sowing (F_{sow}) could potentially enhance European cropland N_2O emissions in 2023 by 0.13 TgN (+35%), whereas N applied at the flowering stage (F_{flower}) could mitigate emissions by 0.08 TgN (-21%). This mitigation occurs in the model because applying additional N at crop flowering, the reproductive stage when plants have the highest N demand, increases N use efficiency, leaving less residual N in the soil to be lost as gaseous emissions. Overall, our uncertainty analysis here suggests that it is possible to find a suitable timing of N fertilization over Europe for N_2O mitigation by aligning fertilizer application with crop growth stages when nitrogen demand is highest. This finding is particularly important for regional application models, as fertilizer data often provide total annual application amounts but typically lack information on seasonal distribution.

Table 3.4.1: *Simulation setups representing different agricultural management scenarios over Europe by LPJ-GUESS.*

Conservation agriculture scenarios					
	CC_L	**CC_{NL}**	**RR**	**NT**	**STD**
Legume cover crop	Yes	No	No	No	No
Non-legume cover crop	No	Yes	No	No	No
Residue retention	25%	25%	100%	25%	25%
Manure application	Yes	Yes	Yes	Yes	Yes
Mineral N fertilizer	Yes	Yes	Yes	Yes	Yes
Tillage	Yes	Yes	Yes	No	Yes
N fertilization management scenarios					
	F_{sow}	**F_{half}**	**F_{flower}**	**-**	**STD**
N applied at sowing	100%	0	0	-	11-50%, depending on crop types
N applied at halfway of the vegetative stage	0	100%	0	-	0-50%, depending on crop types
N applied at flowering	0	0	100%	-	39-50%, depending on crop types

This project has received funding from the European Union's Horizon Europe research and innovation programme under grant agreement No 101081395

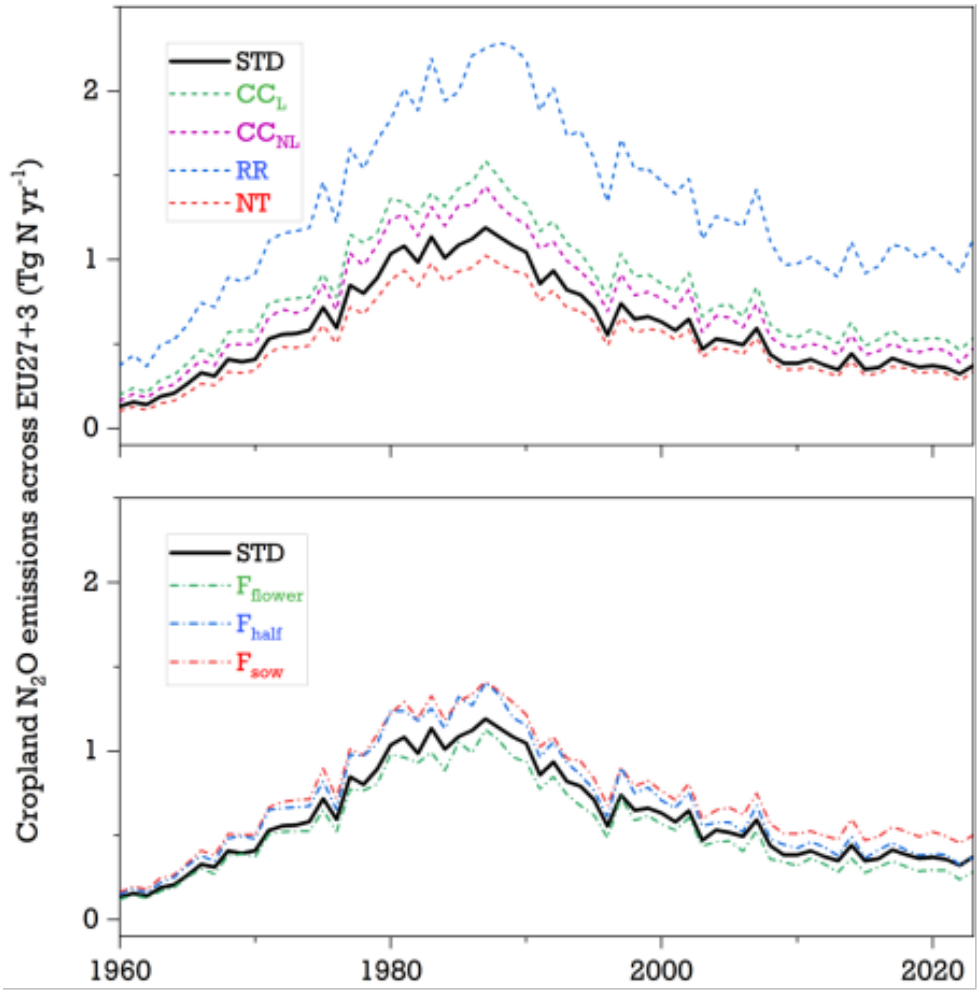

Figure 3.4.1: *Simulated cropland N_2O emissions (TgN yr^{-1}) under different agricultural management scenarios by LPJ-GUESS over EU27+3 countries between 1960-2023.*

4. Process modelling of natural CH_4 fluxes for Europe

4.1 JSBACH-HIMMELI

Natural terrestrial CH_4 flux comprises four terms: peatland soil emission, wet mineral soil emission, dry mineral soil uptake and seasonally inundated soil emission. The peatlands, inundated lands and mineral lands together cover the land area of a grid cell. Peatland extent is considered here as a conservative, static fraction of the grid cell area, and inundated land has variable extent. For methane emission calculations, peatland extent is first subtracted from the inundated land extent (WAD2M, Zhang et al., 2021), and JSBACH-HIMMELI model is used for calculation of peatland fluxes. The remaining inundated land extent is used for calculation of inundated land emissions with a semi-empirical parameterization (Spahni et al, 2011) utilising JSBACH input. The mineral land extent comprises the remains of the grid cell land area after subtracting the joint peatland and inundated land areas, and mineral land fluxes are estimated using approaches by Spahni et al. (2011) and Curry et al. (2017). The land cover input data for methane emission modelling is described in EYE-CLIMA D2.2 including the vegetation and soil type mapping for JSBACH model as well as inundated land maps. The land cover and soil parameterisations were significantly updated from first version using HILDA+ product, which enabled use of high resolution (0.1 x 0.1 degree) data regarding all model land cover inputs also outside EU-27 countries.

This project has received funding from the European Union's Horizon Europe research and innovation programme under grant agreement No 101081395

JSBACH-HIMMELI is a combination of two models, a land-surface model JSBACH (Reick et al 2013), and HIMMELI (HelsinkI Model of MEthane buiLd-up and emIssion for peatlands; Raivonen et al., 2017), which is a specific model for northern peatland emissions of CH_4. JSBACH simulates soil hydrology, vegetation gas exchange and soil carbon input and decay both in oxic and anoxic soil conditions and provides HIMMELI with soil temperature, water table depth, the leaf area index and anoxic respiration from waterlogged soil carbon storages. Decomposition of soil carbon provides substrate for methane production and thus anoxic soil respiration rate is needed to estimate CH_4 fluxes. Simulations of water table level are used for solving the anoxic and oxic layers of the soil column and methane production, oxidation, diffusion and plant transport processes are simulated in those layers.

The parameterisation by Spahni et al (2011) has been applied for calculating methane emissions from the inundated mineral soils, utilising heterotrophic soil respiration rate from JSBACH and a conversion factor for methane emissions. For non-inundated upland mineral soils, the wet mineral soil methane emissions have been calculated using heterotrophic soil respiration rate from JSBACH, a conversion factor for methane, and a rate limitation utilising an empirical soil moisture threshold for mineral soil methane emissions. Dry soil methane uptake rates have been calculated following the Curry (2017) scheme for microbial methane oxidation using soil moisture, soil temperature and soil respiration data produced by JSBACH as input.

CRU-ERA5 climate data have been used to drive JSBACH-HIMMELI in a 0.125 × 0.125 degree resolution grid covering Europe in a rectangular domain (Fig. 4.1.1). JSBACH peat carbon storages were accumulated in a spin-up run. The decay of waterlogged peat is slower than decay of carbon in upland soils and many natural peatlands in northern Europe have been accumulating carbon over a long climate period and currently continue accumulation. For most of the region equilibrium was not reached after 3000 years of spin-up, however at that stage the mean peat depth was around two meters, which is quite realistic for northern European pristine peatlands. Thus, the soil state after 3000 years of spin-up was accepted as the initial state in JSBACH-HIMMELI CH_4 forward simulations, running from year 1990 to 2023. The four methane flux components have been calculated in daily time resolution.

Peatlands

The European peatland methane fluxes are shown as a map in Figure 4.1.1 and as monthly time series over years 1990 – 2023 in Figure 4.1.2. The annual peatland emissions are given together with the other components in Table 4.1.1 and shown as time series in Figure 4.1.3. The distribution of the peatland emissions follows the newly created peatland map based on the Finnish GTK and EU-CORINE and Global GLWDv2 land use maps, as detailed in D2.2 document. Mean annual total maps (Fig. 4.1.1) show less emission in the southern parts of Europe and more emission in the north where peatlands are mostly located, as seen in the high-resolution mapping over the EU27 countries. Total emissions in the domain extending beyond EU27 are smaller than in the first version, probably mostly due to new wetland and land cover maps.

Year-to-year and seasonal variability of the flux components is controlled by meteorological drivers and shows a clear seasonal cycle (Fig. 4.1.2 and Fig 4.1.3). The peatland emissions show high summer-time peak monthly totals, and low winter-time emissions due to freezing temperatures in the north where peatlands are mostly located. The magnitude of the emissions is sensitive to, e.g., simulated peat water table depth, temperature profile and fresh substrate input from peatland vegetation. Peatland emissions are the second largest emission category after inundated land emissions, which has changed since the first version where peatland emissions were largest. There is high year-to-year variability in the summer fluxes. The summer fluxes peaked in 2018 and 2021, while highest yearly fluxes occurred in 2014.

Connecting the year-to-year variability to environmental drivers remains as a future task, as well as studying whether the time series contain any significant trends.

This project has received funding from the European Union's Horizon Europe research and innovation programme under grant agreement No 101081395

Table 4.1.1: *Methane emission components for European domain from JSBACH-HIMMELI in Tg(CH_4)/yr for an area of 35°N to 73°N and 12.1°W to 37.8°E. Mineral soil flux is the total of dry soil uptake and wet soil emission.*

Year	Peatland emission Tg(CH4)/yr	Inundated soil Tg(CH4)/yr	Mineral soil flux Tg(CH4)/yr	Total Tg(CH4)/yr
2000	2.13	2.98	0.47	5.58
2001	2.09	2.85	0.5	5.45
2002	2.25	2.88	0.55	5.68
2003	2.31	2.93	0.25	5.49
2004	2.09	2.92	0.53	5.54
2005	2.21	2.73	0.33	5.27
2006	2.31	2.86	0.49	5.66
2007	2.11	2.88	0.51	5.5
2008	2.03	2.88	0.54	5.45
2009	2.14	3.01	0.52	5.67
2010	2.09	3.15	0.69	5.93
2011	2.22	2.84	0.38	5.44
2012	2.0	3.08	0.61	5.7
2013	2.38	2.9	0.49	5.77
2014	2.4	2.93	0.69	6.02
2015	2.06	2.85	0.22	5.13
2016	2.25	2.98	0.59	5.82
2017	2.06	2.89	0.49	5.44
2018	2.41	3.13	0.3	5.85
2019	2.06	3.28	0.35	5.68
2020	2.29	3.42	0.45	6.16
2021	2.29	2.99	0.42	5.71
2022	2.25	2.92	0.12	5.3
2023	2.22	3.13	0.66	6.01

This project has received funding from the European Union's Horizon Europe research and innovation programme under grant agreement No 101081395

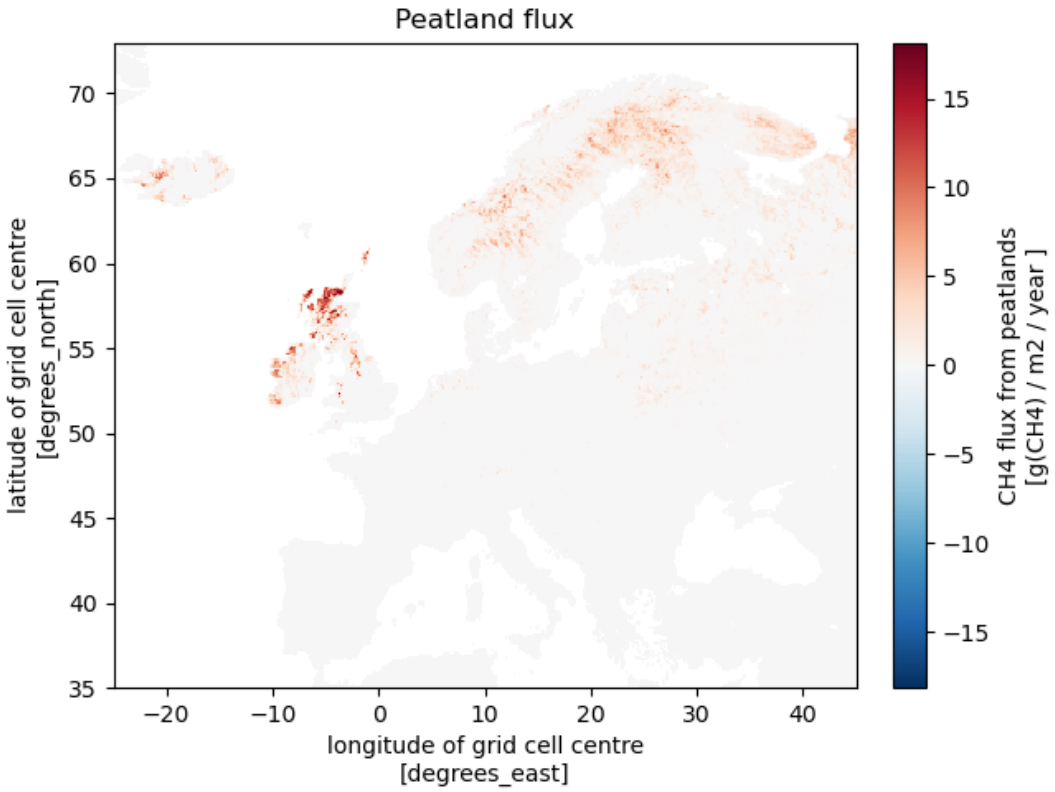

Figure 4.1.1: *Peatland emissions from JSBACH-HIMMELI within the area of EYE-CLIMA European domain. Average over years 1990 – 2023.*

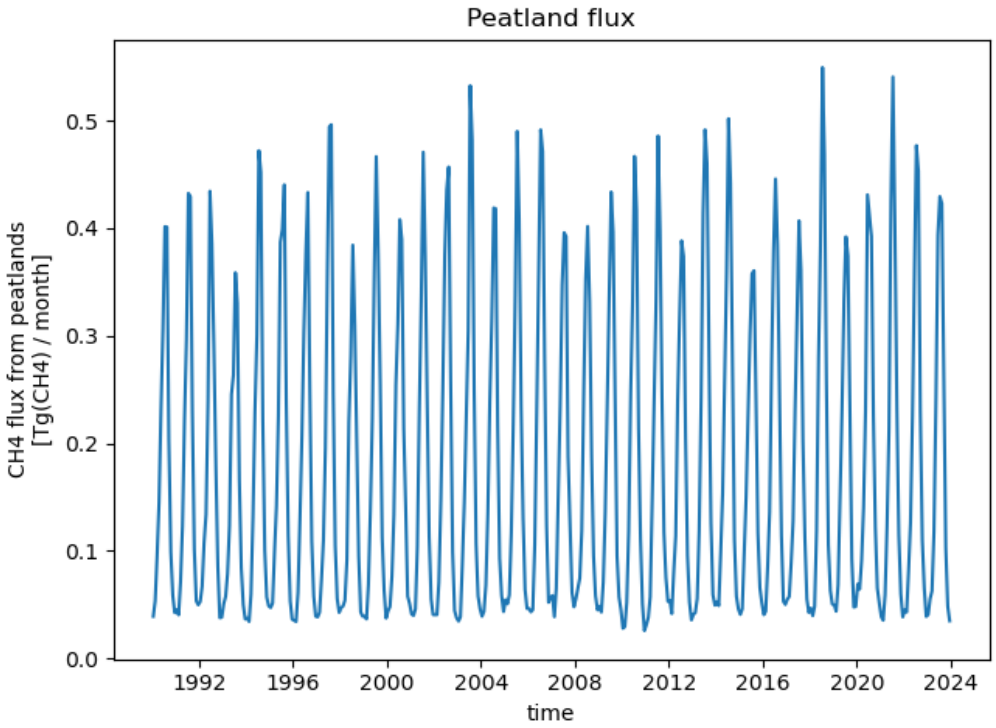

Figure 4.1.2: *Monthly European peatland fluxes from JSBACH-HIMMELI for years 1990 - 2023 in Tg (CH_4)/month.*

This project has received funding from the European Union's Horizon Europe research and innovation programme under grant agreement No 101081395

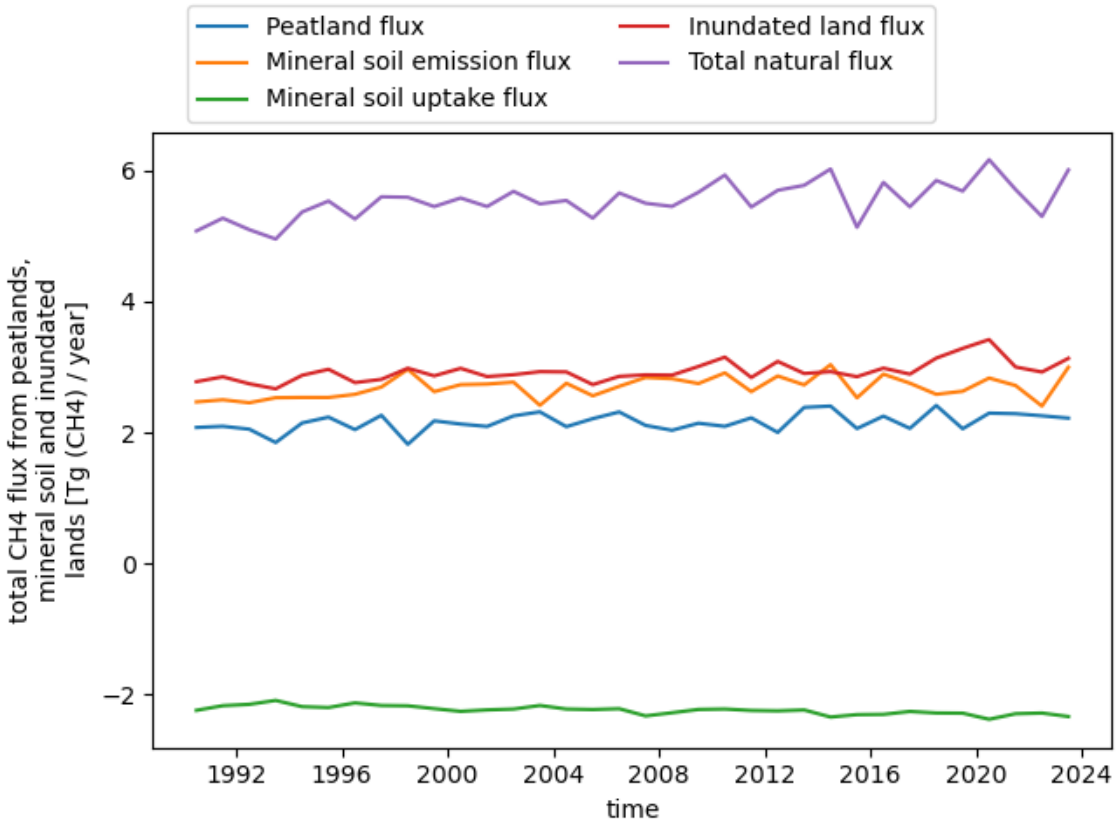

Figure 4.1.3: *Annual total European methane flux components from JSBACH-HIMMELI for years 1990 - 2023 in Tg (CH_4)/month.*

Inundated soils

Inundated areas are located at the low-lying land near lakes, rivers and coastlines. The mean European inundated soil methane fluxes reflect this distribution (Figure 4.1.4) and the variations in fluxes are driven by the heterotrophic soil respiration rate. The inundated soil distribution is dynamic and has high year-to-year and seasonal variation due to precipitation changes and due to snow melt causing spring flooding. This is reflected in monthly inundated soil methane emissions (Figure 4.1.5) as well as in the annual emissions (Table 4.1.1 and Figure 4.1.3). The magnitude of total inundated soil emissions in the EYE-CLIMA domain has doubled since the first version of the deliverable, most likely because of changing to a new land cover outside EU27, which allowed for improved resolution of the grid cell fractions. The year 2020 had the highest inundated soil methane emissions similar to the previous version. High monthly maximum fluxes are present in the later years. Inundated land emissions are a significant contributor to the European terrestrial methane budget, and their temporal variability underlines their importance to be included in the inversion priors.

This project has received funding from the European Union's Horizon Europe research and innovation programme under grant agreement No 101081395

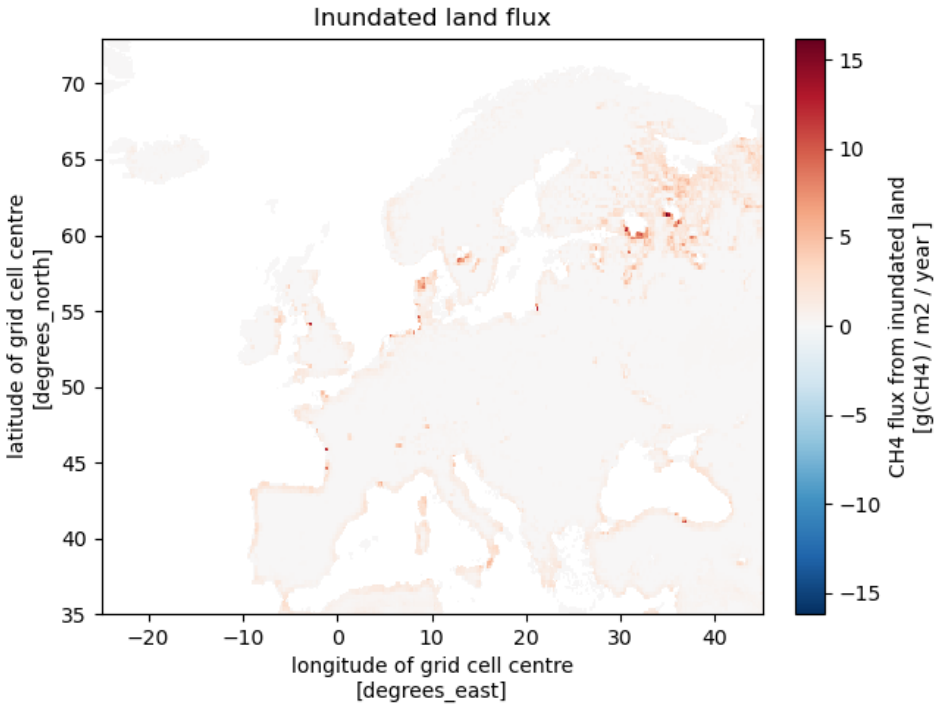

Figure 4.1.4: *Inundated land emissions from JSBACH-HIMMELI within the area of EYE-CLIMA European domain. Average over years 1990 – 2023.*

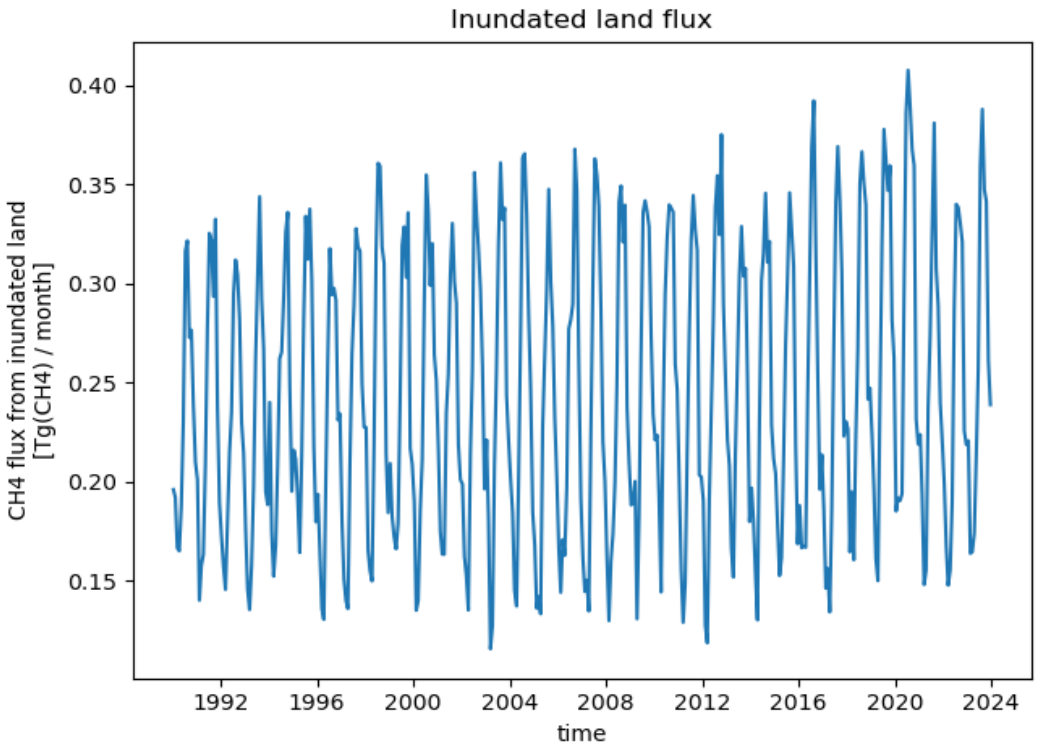

Figure 4.1.5: *Monthly European inundated land fluxes from JSBACH-HIMMELI for years 1990 - 2023 in Tg (CH_4)/month.*

Mineral soils

Mineral soil emissions include both dry mineral soil uptake and wet mineral soil emissions. These components are added together and the annual average mineral soil fluxes are given in Table 4.1.1. The average fluxes suggest methane emission by mineral soils every year, in contrast to the first version of

This project has received funding from the European Union's Horizon Europe research and innovation programme under grant agreement No 101081395

the deliverable. The map over Europe (Figure 4.1.6) shows that the emissions occur in regions with high precipitation, along coastlines and mountainous regions and that there are complex patterns of emissions across Europe where there used to be sinks earlier. The moisture content of the soils is higher than previously. The new climate drivers might lead to an increase in soil moisture or the new land cover and soil descriptions better retain moisture in the soil. Increased soil moisture increases soil respiration and provides more substrate for methane production in oxygen-poor conditions. The time series of the dry mineral soil and wet mineral soil flux components are presented in Fig 4.1.3, which shows that the dry mineral soil year-to-year variability is modest. Variability in wet mineral soil fluxes is larger, with highest emissions in year 2014, similarly to peatlands. The combined mineral soil fluxes are smaller than peatland and inundation emissions, but they still contribute by a significant amount to the total budget. The month-to-month variability of the fluxes (Figure 4.1.7) is quite large due to soil moisture changes from winter to summer seasons and due to precipitation changes.

Total methane emissions including all components are shown in Figure 4.1.8. They are higher than in the first version probably due to increased soil moisture, changes in vegetation and surface property values and higher resolution in land cover (HILDA) outside the EU27 countries in Eastern Europe, which allows for more accurate grid cell fractions for the emission components and their local variability.

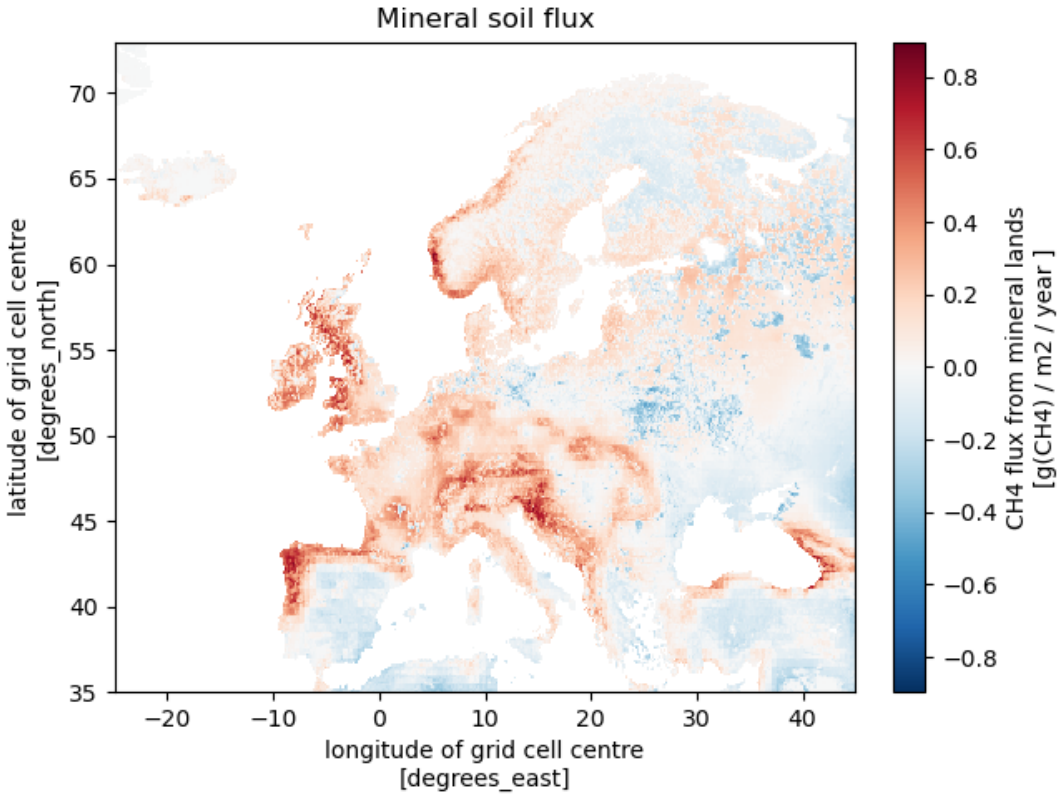

Figure 4.1.6: *Mineral soil fluxes from JSBACH-HIMMELI within the area of EYE-CLIMA European domain. Average over years 1990 – 2023.*

This project has received funding from the European Union's Horizon Europe research and innovation programme under grant agreement No 101081395

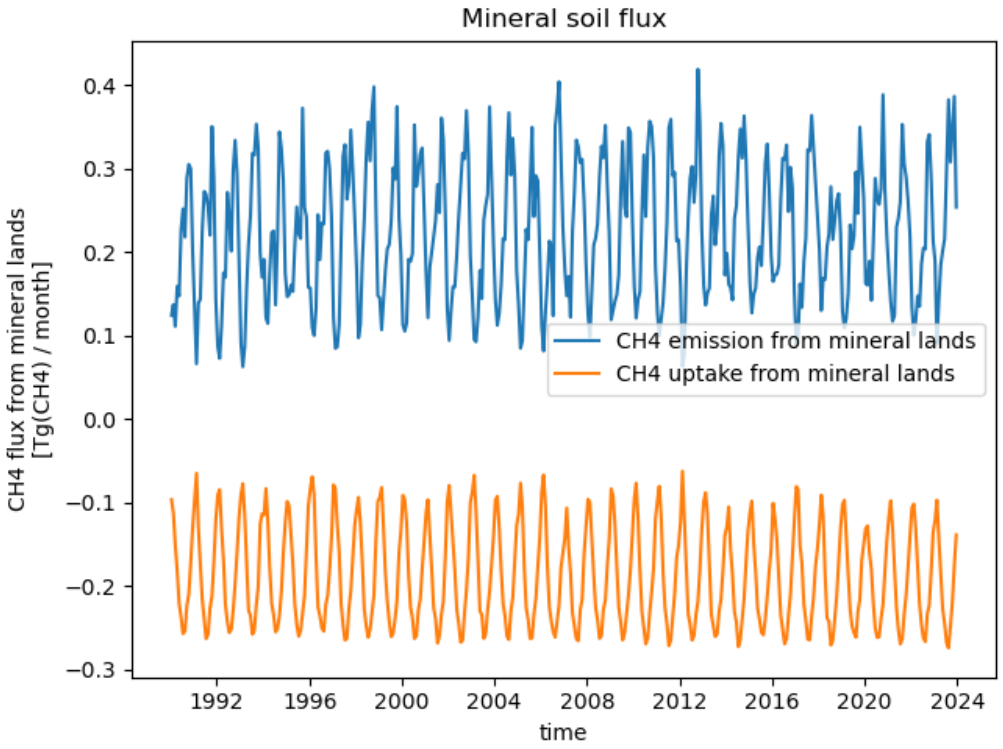

***Figure 4.1.7**: Monthly European mineral soil fluxes from JSBACH-HIMMELI for years 1990 - 2023 in Tg (CH_4)/month.*

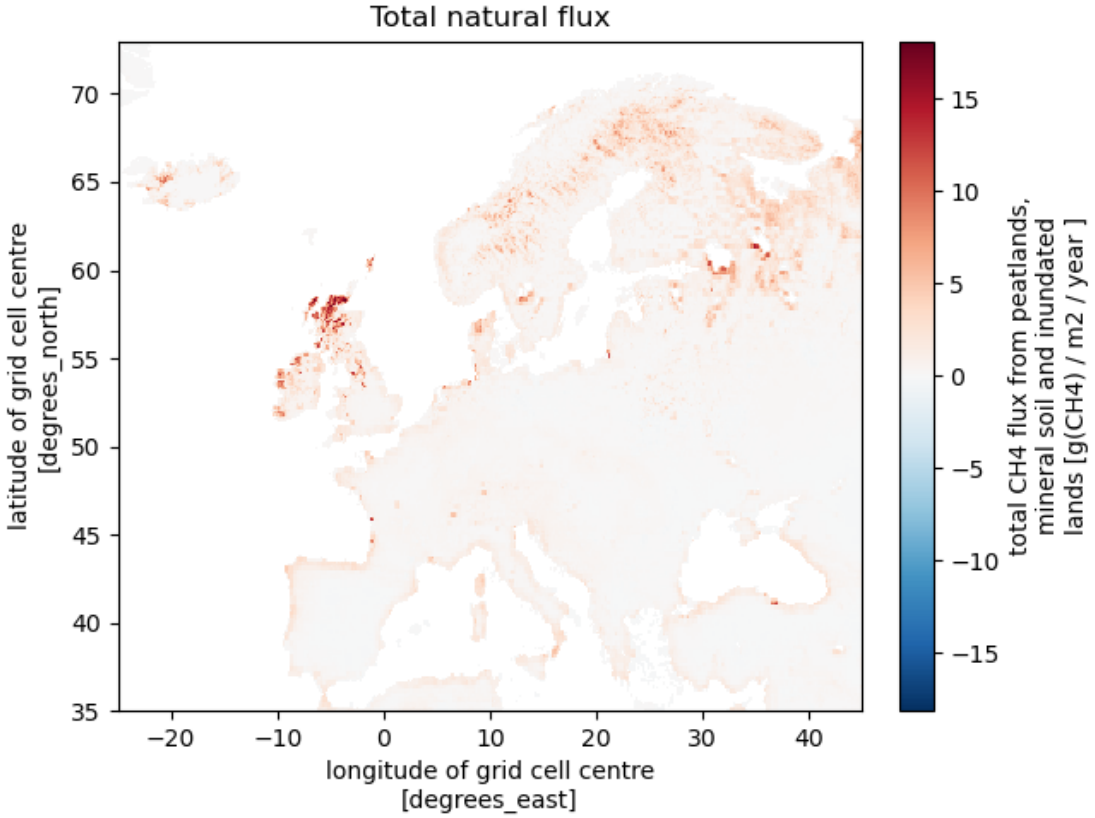

***Figure 4.1.8:** Total biospheric methane fluxes from JSBACH-HIMMELI within the area of EYE-CLIMA European domain. Average over years 1990 – 2023.*

This project has received funding from the European Union's Horizon Europe research and innovation programme under grant agreement No 101081395

4.2 ORCHIDEE

Model description for the CH_4 fluxes

A different version of ORCHIDEE than the one used for CO_2 and N_2O fluxes has been employed for this second round of simulations. It is based on the ORCHIDEE-PEAT version, described in Salmon et al. (2022) and further updated in Liu et al. (2025). ORCHIDEE-PEAT integrates the peatland soil hydrology to simulate waterlogged conditions, process-based module for soil temperature that simulates soil freezing, thawing and phase change-induced heat fluxes in the soil, a photosynthesis scheme of a mixed plant species northern peatland ecosystem and a scheme of peat accumulation and decomposition to CO_2 for three soil carbon pools: active, slow and passive, which are vertically discretized (Qiu et al., 2019).

The methane scheme includes: 1) methanogenesis of the three carbon pools, 2) methane and oxygen transport in the soil and snow layers, 3) transport of methane to the atmosphere by ebullition, 4) plant mediated transport and 5) methanotrophy by soil oxic conditions and roots exudates. The model was calibrated and evaluated on 14 northern peatland sites distributed on both the Eurasian and American continents in the northern boreal and temperate regions. Data assimilation approaches were employed to optimise parameters at all sites simultaneously. The model simulates methane emissions from peatlands and inundated soils as well as from mineral soils.

The model has then been updated by Liu et al. (2025) by incorporating three new peatland-specific plant functional types (PFTs), namely deciduous broadleaf shrub, moss and lichen, as well as evergreen needleleaf tree in addition to previously peatland graminoid PFT to simulate peatland vegetation dynamic and soil CH_4 and CO_2 fluxes. Model parameters controlling photosynthesis, autotrophic respiration, and carbon decomposition have also been optimized using eddy-covariance observations from 14 European peatlands and a Bayesian optimization approach. CH_4 fluxes simulated with this updated model version (compared to the previous set of fluxes based on the version of Salmon et al., (2022)) are presented below.

Note that, unfortunately, the coupling of these methane-specific developments into the trunk version of ORCHIDEE, to have a comprehensive set of fluxes (including CO_2, CH_4 and N_2O) is still in progress, due to unforeseen complex technical difficulties, mainly because of the addition of the nitrogen cycle in trunk version that was not included the ORCHIDEE-PEAT version. In addition, we could not easily re-run the initial ORCHIDEE-PEAT version with the new high resolution climate forcing, given some changes in the overall code management software, linked to the need of running in parallel mode at high resolution.

In this context, we thus provide below an analysis of the ORCHIDEE-PEAT model simulation, that was run at a coarser resolution (at 1°). These fluxes only cover the period 2000 to 2022 and will thus only potentially be used as a climatology for the atmospheric inversion and the overall CH_4 synthesis. However, a simulation at high resolution with the selected forcing (ERA5land + CRU) should be available in spring 2026 with this model version; it will thus be used to update the first comparison with JSBACH-HIMMELI fluxes (see section 4.3) and it will potentially serve as prior for atmospheric inversion tests (compared to using JSBACH-HIMMELI).

Flux estimates

Figure 4.2.1 and Table 4.2.1 provide an illustration of the spatial and temporal distribution of the simulated CH_4 emissions with the ORCHIDEE-PEAT model version at coarse resolution and only over the period 2000 - 2022. Like with JSBACH-HIMMELI, the maximum CH_4 emissions are located in northern Europe and to a lesser extent northern United Kingdom. The differences in spatial resolution between the two model simulations prevent a much more in-depth comparison of the spatial distribution. With respect to the temporal evolution, Figure 4.2.1 shows a large positive trend in CH_4 emissions over the two decades, with large year-to-year variations. For instance, we notice high emissions in 2007, 2014

This project has received funding from the European Union's Horizon Europe research and innovation programme under grant agreement No 101081395

and 2018 for ORCHIDEE-PEAT. These maximums do not correspond to maximum emissions with JSBACH-HIMMELI, due to different wetland extent dynamics, climate forcing and model structure. We will investigate more deeply the driver of the model differences, once the simulation at high resolution with ORCHIDEE-PEAT will be performed.

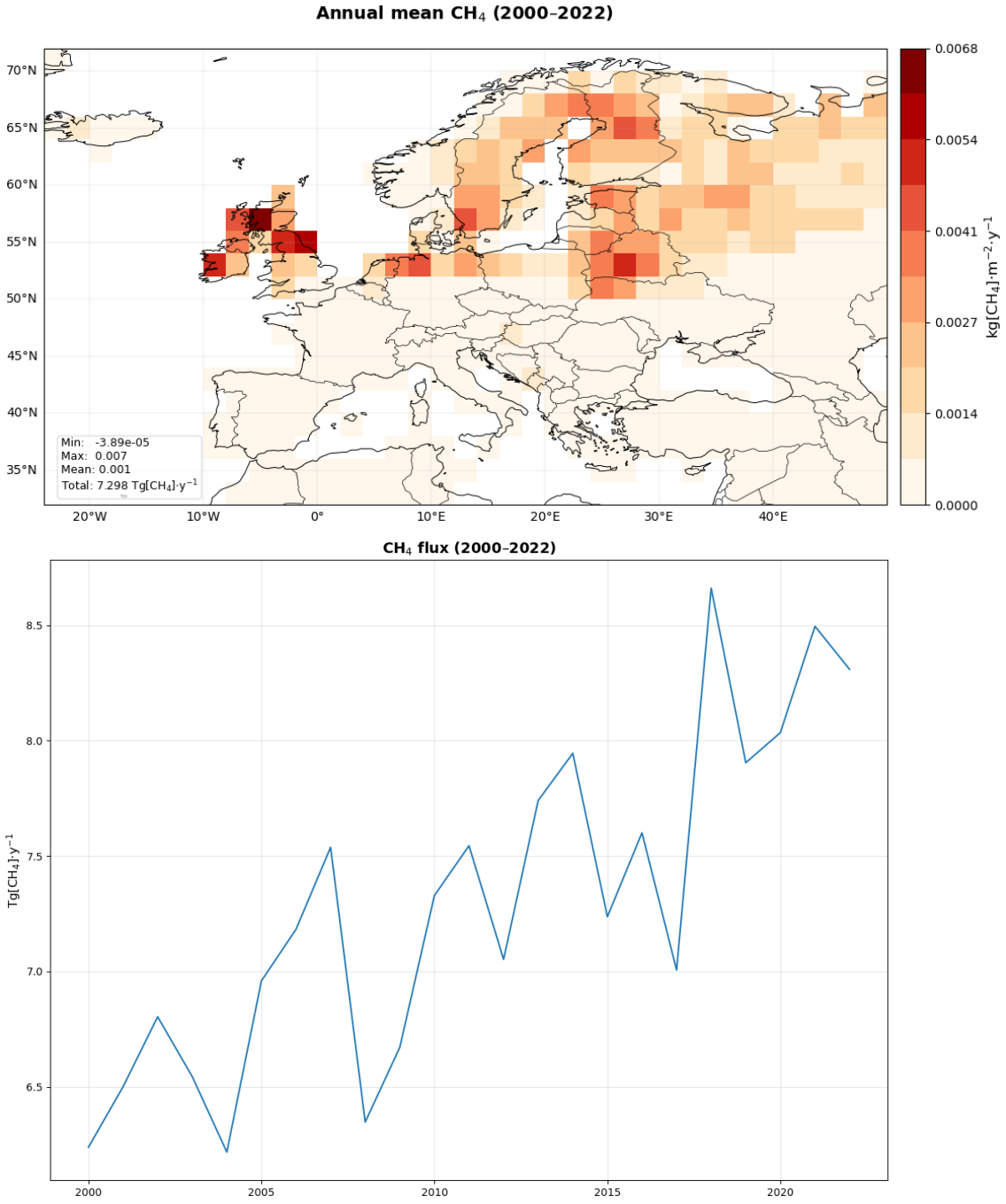

Figure 4.2.1: *Top: Map of the annual methane emission from peatland from ORCHIDEE in kgCH_4/m^2/yr. Bottom: temporal evolution of these methane emissions for an area of 35°N to 73°N and 12.1°W to 37.8°E.*

This project has received funding from the European Union's Horizon Europe research and innovation programme under grant agreement No 101081395

Table 4.2.1: *Methane emission components for the European domain from ORCHIDEE in Tg(CH_4)/yr for an area of 35°N to 73°N and 12.1°W to 37.8°E. It includes the total Peatland plus inundated soil emission as well as the absorption from mineral soils.*

Year	Peatland emission + inundated soil (units Tg(CH_4)/yr)
2000	6.2382
2001	6.5000
2002	6.8034
2003	6.5446
2004	6.2172
2005	6.9591
2006	7.1824
2007	7.5377
2008	6.3474
2009	6.6712
2010	7.3286
2011	7.5447
2012	7.0519
2013	7.7406
2014	7.9450
2015	7.2368
2016	7.6007
2017	7.0058
2018	8.6600
2019	7.9040
2020	8.0345
2021	8.4951
2022	8.3087
Mean	7.2982

4.3 Comparison between ORCHIDEE and JSBACH-HIMMELI CH_4 fluxes

We present a first comparison between the two models, although they are not run at the same spatial resolution and with the same meteorological forcing. The total European terrestrial methane emissions show different levels and deviating trends through the common simulation period 2000-2022 (Fig 4.3.1).

This project has received funding from the European Union's Horizon Europe research and innovation programme under grant agreement No 101081395

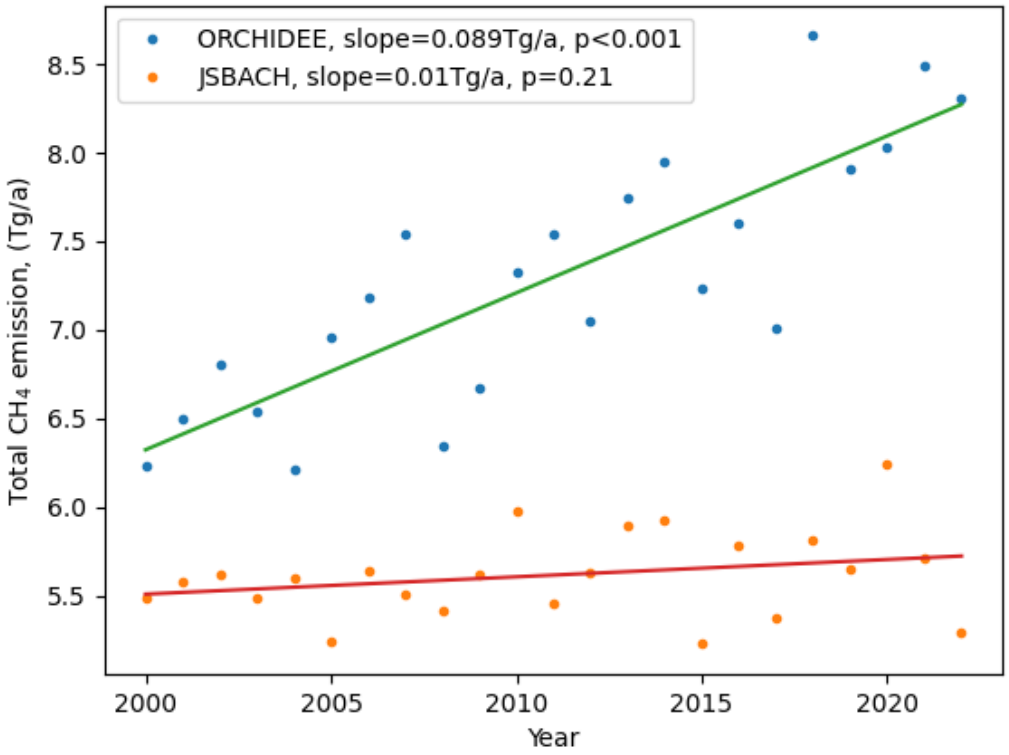

Figure 4.3.1. *Annual European methane emission through 2000-2022 from OCHIDEE and JSBACH ecosystem models.*

The reasons for the deviating trends were inspected by looking at the trends of seasonal component fluxes and their meteorological drivers. JSBACH total flux is comprised of emissions from peatlands, from wet mineral soils and from seasonal inundated fraction of the grid-cells and uptake by dry mineral soils. ORCHIDEE has sixteen vegetation type specific layers out of which classes 14 to 16 represent peatlands and show most prominent emissions, whereas the classes 1 to 13 show uptake. The partitioning of the fluxes to their main components revealed that ORCHIDEE's large emission trend is mainly due to summertime fluxes of peatlands (Fig 4.3.2). The respective flux component from JSBACH showed only insignificant positive emission trends while the significant peatland emission trends were tiny and negative. The largest positive (p>0.01) trends were observed in Scandinavia, Scotland and Ireland.

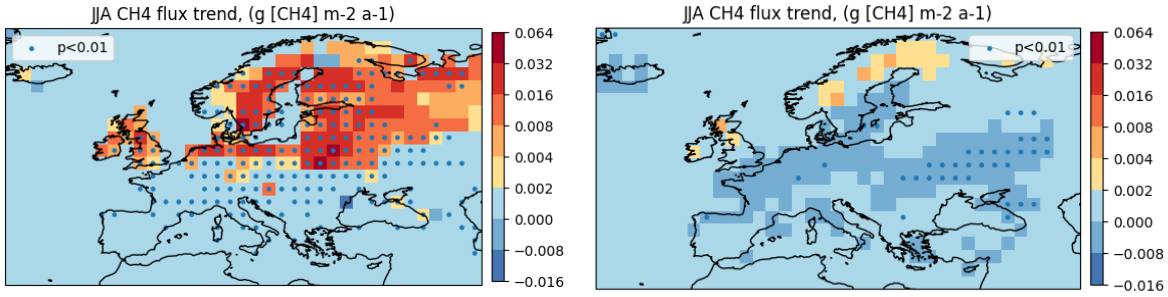

Figure 4.3.2. *Spatial distributions of summertime (JJA) peatland emissions trends from ORCHIDEE (left) and JSBACH (right).*

This project has received funding from the European Union's Horizon Europe research and innovation programme under grant agreement No 101081395

Because the models were driven with different meteorological data products, we compared the trends of air temperature and precipitation between both data. The spatial distributions of the seasonal trends and as well as their significance agreed well for daily minimum and maximum air temperatures and precipitation (not shown). CRUERA_v5 typically showed slightly stronger trends and somewhat larger continuous areas of significance. However, because ORCHIDEE showed the large peatland emission trend we concentrate on its driving data source CRUJRA2.4.5, in what follows.

CRUJRA2.4.5. did not have any significant precipitation trend within the region of the large peatland emission trend (Fig. 4.3.3). Overall, in most of the regions of positive summertime CH_4 emission trends (Fig. 4.3.2), precipitation shows negative summertime trend (except east of Finland). The most outstanding exceptions are the north-eastern parts of the domain extending from mid-Finland towards the region surrounding the White Sea in north-western Russia, where the strong significant positive summertime CH_4 flux trends coincide with positive precipitation trends.

Summertime maximum air temperature trends are positive throughout Europe (Fig. 4.3.3) but strongest in the middle of the domain overlapping with the grid-cells with the highest CH_4 emission trends. However, the trends are much weaker and less significant in most of the regions of CH_4 emission increase. Minimum air temperature shows even weak negative trends in the middle of the domain (not shown) but not in the areas of CH_4 positive trends.

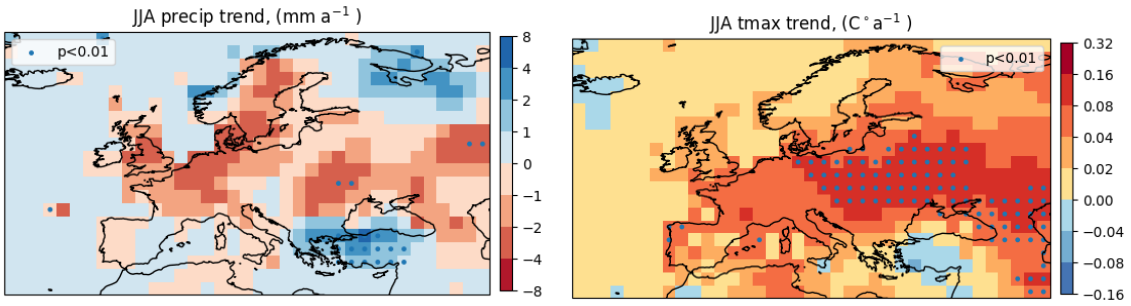

Figure 4.3.3. *CRUJRA-2.4.5 summertime (JJA) precipitation (left) and maximum air temperature (right) trends through 2000-2022.*

Overall, the ORCHIDEE's large positive methane emission trends coincide with increasing maximum air temperature trend and for most of the region with decreasing precipitation trends. JSBACH's drivers have even stronger trends but the model's response is much more modest and for part of the domain, even of different signs. Thus, ORCHIDEE's CH_4 emissions seem to be more sensitive especially to the trends in air temperature.

4.4 Uncertainties

Wetlands

The European terrestrial methane emissions contain many uncertainties related to climate drivers, land cover, inundated area, peatland process model parameters, mineral soil parameterizations and model structures etc. Uncertainties due to model structures can be estimated by considering more than one model.

For land cover, the uncertainties are related to plant functional type distributions and soil type descriptions affecting the soil moisture and soil water table level as well as amount of substrate for methane production. Inundated area, when using a prescribed satellite-product, has uncertainties due to possible overlap with lakes and other water bodies, and forests obstructing the view to inundated

This project has received funding from the European Union's Horizon Europe research and innovation programme under grant agreement No 101081395

surface. Mineral soil emissions are very uncertain due to limited information on moisture threshold for methane emission, sensitivity to climate drivers and challenges with soil moisture simulations.

Sensitivity to wetland area was tested by using different static and monthly varying wetland datasets (Figure 4.3.1). For the EU27 region, Corine+GTK static wet peatlands + monthly inundation from WAD2M in the basic set-up was replaced by GLWDv2 static wet peatlands + monthly inundation from GIEMS2. Outside EU27 the difference comes from WAD2M versus GIEMS2. Largest uncertainties (relative to average flux) are linked to the inundation extent especially during snow melt/high precipitation months. However, further analysis is needed with a larger number of wetland datasets.

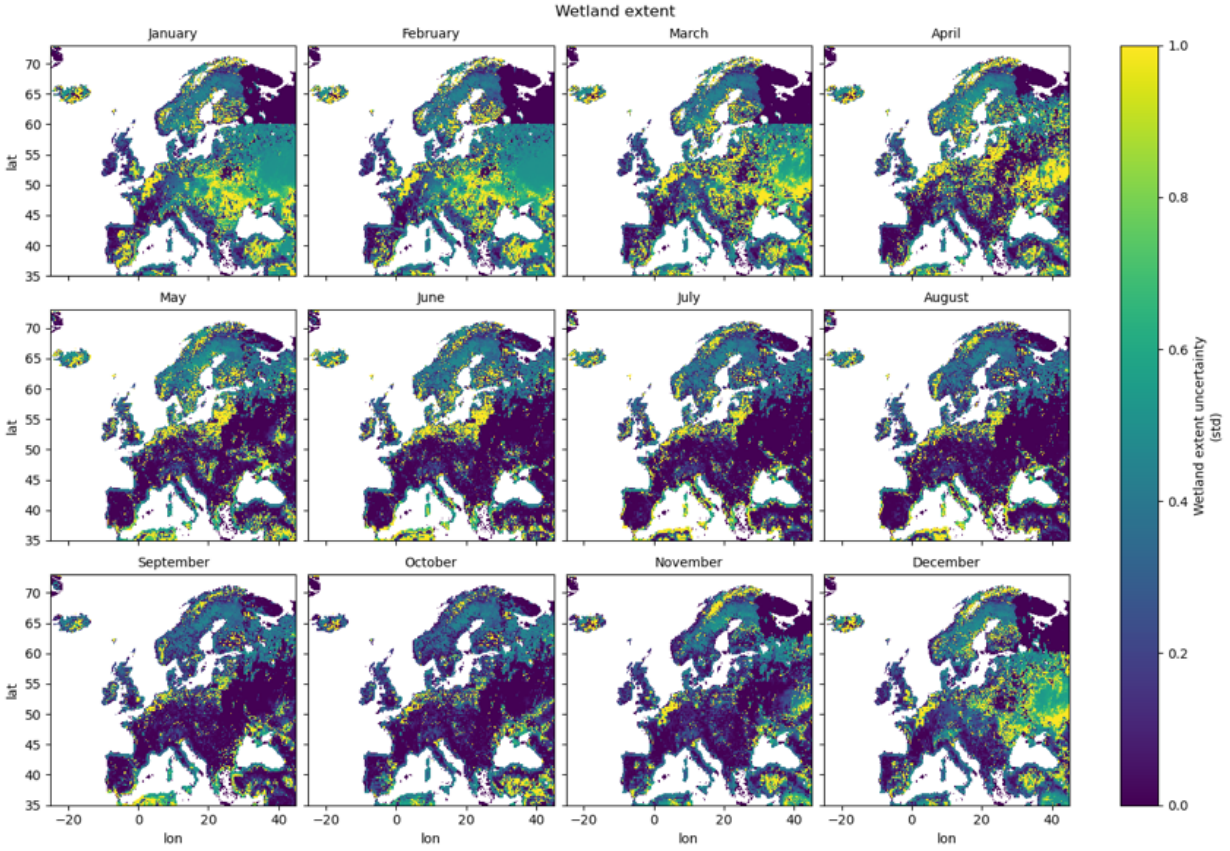

Figure 4.3.1: *Monthly uncertainties relative to mean European methane fluxes estimated with JSBACH-HIMMELI over years 1990-2023, using different land cover data sets for wetland extent.*

Differences in climate drivers can lead to significant differences in European methane budgets, and thus the impact of the driver data was considered in the sensitivity analysis. The driver datasets may have differences in daily / monthly aggregated values as well as in long term trends. Results from two driver datasets (CRU-HARMONIE, CRU-ERA) are shown in Figure 4.3.2 for methane emissions. Uncertainties (relative to the average flux) are highest in the region of lowest emissions outside the peatland-rich areas and outside the summer months. However, they might be somewhat overestimated and further analysis is needed with more data.

This project has received funding from the European Union's Horizon Europe research and innovation programme under grant agreement No 101081395

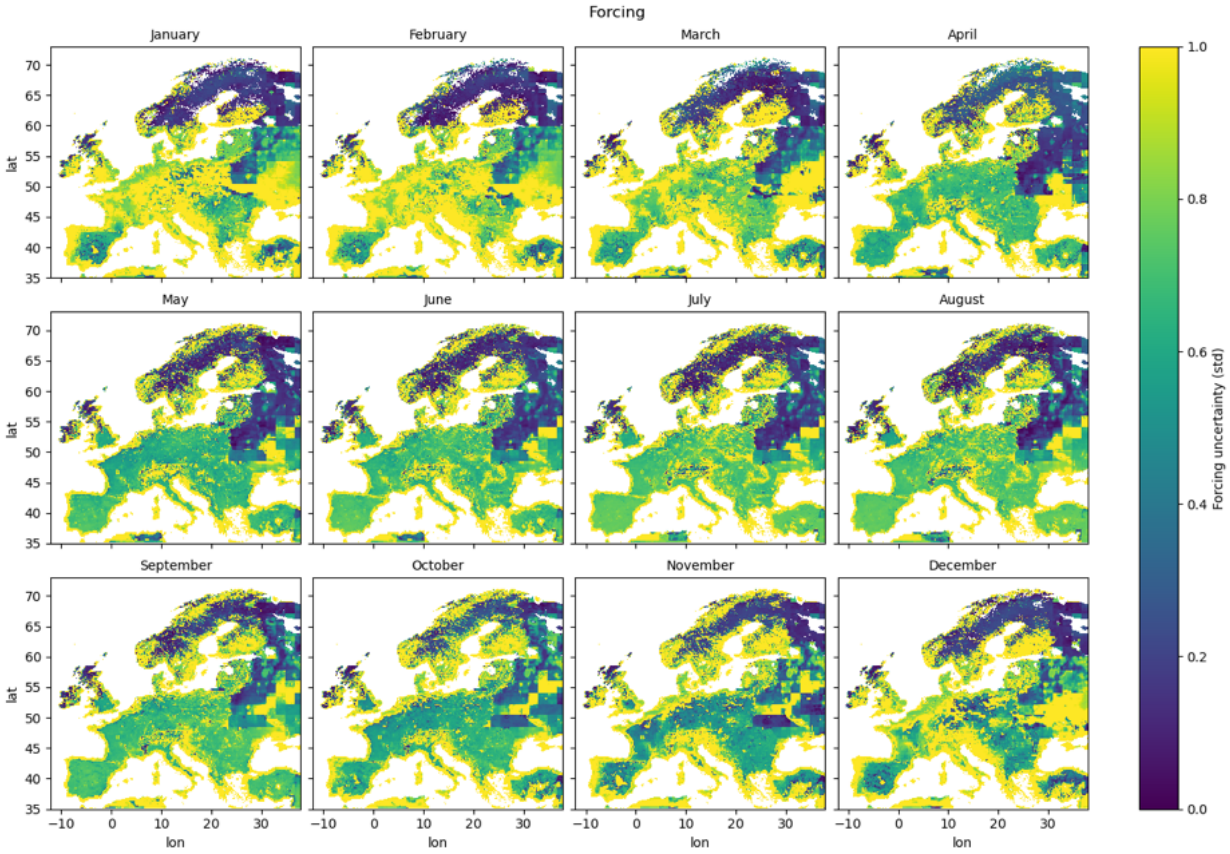

Figure 4.3.2: *Monthly uncertainties relative to mean European methane fluxes estimated with JSBACH-HIMMELI over years 1990-2023, using CRU-HARMONIE or CRU-ERA climate data as input.*

Peatland process parameters have been optimized previously for individual sites (e.g., Susiluoto et al., 2018, Gao et al., 2025), and those optimised parameter value distributions were taken into use in regional simulations for estimating the European scale flux uncertainties. Parameter values for each key methane process (production, plant transport, oxidation) were varied according to results by Susiluoto et al (2018) and Gao et al. (2025) and European methane fluxes were produced with JSBACH-HIMMELI. Flux responses to changes in parameter values were non-linear and had latitudinal dependencies. Standard deviation of parameter combinations was chosen to describe the parametric uncertainty range in methane fluxes, and uncertainty was calculated relative to mean fluxes (Figure 4.3.3).

This project has received funding from the European Union's Horizon Europe research and innovation programme under grant agreement No 101081395

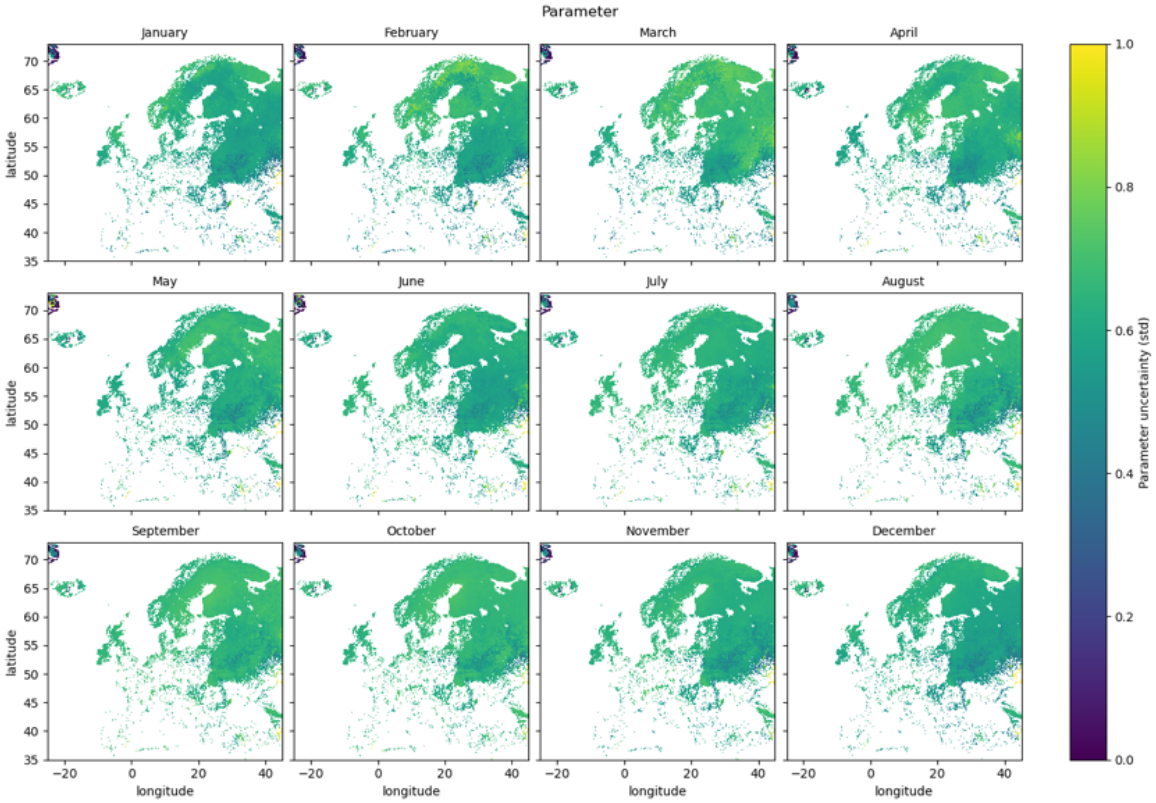

Figure 4.3.3: *Monthly uncertainties in European methane fluxes estimated with JSBACH-HIMMELI over years 1990-2023, using different HIMMELI parameter values as input.*

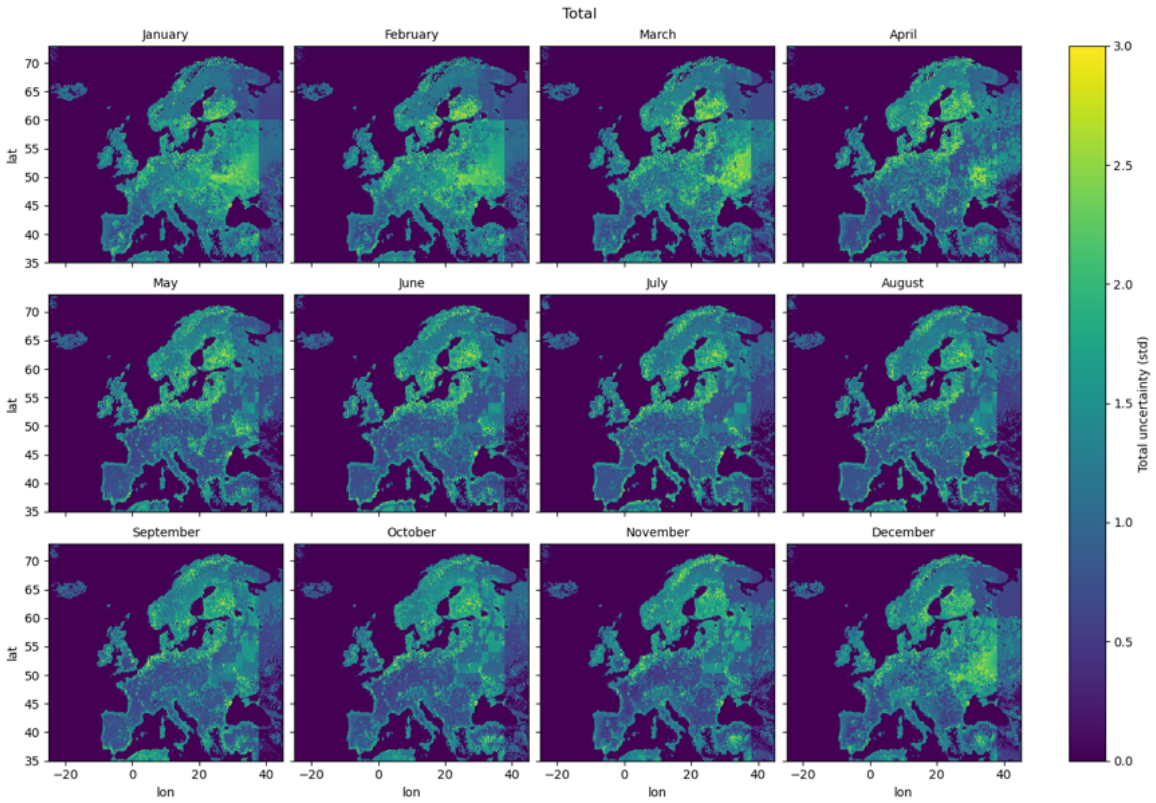

Figure 4.3.4: *Monthly uncertainties in European methane fluxes estimated with JSBACH-HIMMELI over years 1990-2023.*

This project has received funding from the European Union's Horizon Europe research and innovation programme under grant agreement No 101081395

The three components were added together for total uncertainty (Figure 4.3.4). In the future, studies will need to be continued to investigate in more detail the role of the different components in the overall uncertainty, and guidelines need to be prepared for estimation of the regional simulation uncertainties in order to consistently use them in atmospheric inversions together with the other prior uncertainty sources.

5. Conclusions

Carbon dioxide, methane and nitrous oxide balances of terrestrial ecosystems have been produced using three process-based models (ORCHIDEE, LPJ-GUESS and JSBACH-HIMMELI, using two models for each species). The carbon dioxide flux products cover Europe over years 1901-2023, nitrous oxide results over years 1901 – 2023 and methane balance products for years 1990-2023. The flux estimates will be used as prior data in the atmospheric inversion modelling task in WP3 and for synthesis of national GHG budgets in WP4. The applied aerial domains as well as time coverages and resolutions may limit the applicability of the products. Significant differences are obtained between the selected models depending on the species. For CO_2, the net annual carbon flux simulated by LPJ-GUESS and ORCHIDEE have similar magnitudes; the year-to-year variations are also well correlated between the two models. For N_2O, we obtain larger differences with little year-to-year flux correlations and a large difference in the trend of the N_2O emissions over cropland (a decreasing trend in LPJ-GUESS not present in ORCHIDEE). For CH_4, unfortunately the ORCHIDEE simulation could not be performed with the same high-resolution climate forcing as JSBACH-HIMMELI; overall JSBACH-HIMMELI provides lower fluxes than ORCHIDEE with also a lower positive trend over Europe. The comparison between these models is still ongoing with more in-depth analysis of the causes of the differences. Note also that these simulated fluxes correspond to the second round of model simulations, and to the final version of this deliverable.

This project has received funding from the European Union's Horizon Europe research and innovation programme under grant agreement No 101081395

6. References

Batjes, N. H. (2016). Harmonized soil property values for broad-scale modelling (WISE30sec) with estimates of global soil carbon stocks. Geoderma, 269, 61–68. https://doi.org/10.1016/j.geoderma.2016.01.034

Blanc-Betes, E., Kantola, I. B., Gomez-Casanovas, N., Hartman, M. D., Parton, W. J., Lewis, A. L., et al. (2021). In silico assessment of the potential of basalt amendments to reduce N2O emissions from bioenergy crops. GCB Bioenergy, 13(1), 224–241. https://doi.org/10.1111/gcbb.12757

Cleveland, C. C., Townsend, A. R., Schimel, D. S., Fisher, H., Howarth, R. W., Hedin, L. O., ... & Wasson, M. F. (1999). Global patterns of terrestrial biological nitrogen (N2) fixation in natural ecosystems. Global biogeochemical cycles, 13(2), 623-645, https://doi.org/10.1029/1999GB900014

Collatz, G. J., Ribas-Carbo, M., & Berry, J. A. (1992). Coupled photosynthesis-stomatal conductance model for leaves of C4 plants. Functional Plant Biology, 19(5), 519-538,

De Rosnay, P., Polcher, J. D., Bruen, M., & Laval, K. (2002). Impact of a physically based soil water flow and soil-plant interaction representation for modeling large-scale land surface processes. Journal of Geophysical Research: Atmospheres, 107(D11), ACL-3, https://doi.org/10.1029/2001JD000634.

d'Orgeval, T., Polcher, J., & De Rosnay, P. (2008). Sensitivity of the West African hydrological cycle in ORCHIDEE to infiltration processes. Hydrology and Earth System Sciences, 12(6), 1387-1401, https://doi.org/10.5194/hess-12-1387-2008

Farquhar, G. D., von Caemmerer, S. V., & Berry, J. A. (1980). A biochemical model of photosynthetic CO2 assimilation in leaves of C3 species. planta, 149(1), 78-90, .

Friedlingstein, P., Jones, M. W., O'Sullivan, M., Andrew, R. M., Bakker, D. C., Hauck, J., ... & Zeng, J. (2022). Global carbon budget 2021. Earth system science data, 14(4), 1917-2005, https://doi.org/10.5194/essd-14-1917-2022

Gao, Y., Burke, E. J., Chadburn, S. E., Raivonen, M., Markkanen, T., Aurela, M., Flanagan, L. B., Fortuniak, K., Humphreys, E., Lohila, A., Li, T., Mammarella, I., Nevalainen, O., Nilsson, M. B., Pawlak, W., Tsuruta, A., Yang, H., and Aalto, T.: Assessing modelled methane emissions over northern wetlands by the JULES-HIMMELI model, Science of The Total Environment, 980, 179526,https://doi.org/10.1016/j.scitotenv.2025.179526, 2025.

Joiner, J., Yoshida, Y., Zhang, Y., Duveiller, G., Jung, M., Lyapustin, A., ... & Tucker, C. J.: Estimation of terrestrial global gross primary production (GPP) with satellite data-driven models and eddy covariance flux data. Remote Sensing, 10(9), 1346, 2018, https://doi.org/10.3390/rs10091346.

Krinner, G., Nicolas, V., de Noblet-Ducoudre, N., Ogée, J., Polcher, J., Friedlingstein, P., Ciais, P., Sitch, S., and Prentice, I.: A dynamic global vegetation model for studies of the coupled atmosphere-biosphere system, Global Biogeochemical Cycles, 19, GB1015, https://doi.org/10.1029/2003GB002199, 2005

Li, C., Aber, J., Stange, F., Butterbach-Bahl, K., and Papen, H.: A process-oriented model of N_2O and NO emissions from forest soils: 1. Model development, J. Geophys. Res.-Atmos., 105, 4369–4384, https://doi.org/10.1029/1999JD900949, 2000

Lindeskog, M., Arneth, A., Bondeau, A., Waha, K., Seaquist, J., Olin, S., & Smith, B. (2013). Implications of accounting for land use in simulations of ecosystem carbon cycling in Africa. Earth System Dynamics, 4(2), 385–407. https://doi.org/10.5194/esd-4-385-2013

Lindeskog, M., Smith, B., Lagergren, F., Sycheva, E., Ficko, A., Pretzsch, H., & Rammig, A. (2021). Accounting for forest management in the estimation of forest carbon balance using the dynamic

This project has received funding from the European Union's Horizon Europe research and innovation programme under grant agreement No 101081395

vegetation model LPJ-GUESS (v4.0, r9710): Implementation and evaluation of simulations for Europe. Geoscientific Model Development (Vol. 14). https://doi.org/10.5194/gmd-14-6071-2021

Liu, B., Mørkved, P. T., Frostegård, Å., & Bakken, L. R. (2010). Denitrification gene pools, transcription and kinetics of NO, N2O and N2 production as affected by soil pH. FEMS Microbiology Ecology, 72(3), 407–417. https://doi.org/10.1111/j.1574-6941.2010.00856.x

Liu, L., Qiu, C., Xi, Y., Salmon, E., Kalhori, A., Artz, R. R., ... & Ciais, P. (2025). Assessing CO2 fluxes for European peatlands in ORCHIDEE-PEAT with multiple plant functional types. Journal of Advances in Modeling Earth Systems, 17(6), e2025MS004940, https://doi.org/10.1029/2025MS004940 .

Lurton, T., Balkanski, Y., Bastrikov, V., Bekki, S., Bopp, L., Braconnot, P., ... & Boucher, O. (2020). Implementation of the CMIP6 forcing data in the IPSL-CM6A-LR model. Journal of Advances in Modeling Earth Systems, 12(4), e2019MS001940.

Lugato, E., Leip, A., & Jones, A. (2018). Mitigation potential of soil carbon management overestimated by neglecting N2O emissions. Nature Climate Change, 8(3), 219–223. https://doi.org/10.1038/s41558-018-0087-z

Ma, J., Olin, S., Anthoni, P., Rabin, S. S., Bayer, A. D., Nyawira, S. S., & Arneth, A. (2022). Modeling symbiotic biological nitrogen fixation in grain legumes globally with LPJ-GUESS (v4.0 , r10285). Geoscientific Model Development, 15(2), 815–839. https://doi.org/10.5194/gmd-15-815-2022

Ma, J., Arneth, A., Smith, B., Anthoni, P., Xu-Ri, Eliasson, P., et al. (2024). Soil nitrous oxide emissions from global land ecosystems and their drivers within the LPJ-GUESS model (v4.1). Geoscientific Model Development Discussion. https://doi.org/10.5194/gmd-2024-223

Maag, M., & Vinther, F. P. (1996). Nitrous oxide emission by nitrification and denitrification in different soil types and at different soil moisture contents and temperatures. Applied Soil Ecology, 4, 5–14.

Mei, K., Wang, Z., Huang, H., Zhang, C., Shang, X., Dahlgren, R. A., et al. (2018). Stimulation of N2O emission by conservation tillage management in agricultural lands: A meta-analysis. Soil and Tillage Research, 182(March), 86–93. https://doi.org/10.1016/j.still.2018.05.006

Meinshausen, M., Nicholls, Z. R. J., Lewis, J., Gidden, M. J., Vogel, E., Freund, M., et al. (2020). The shared socio-economic pathway (SSP) greenhouse gas concentrations and their extensions to 2500. Geoscientific Model Development, 13(8), 3571–3605. https://doi.org/10.5194/gmd-13-3571-2020

Nelson, J. A., Walther, S., Gans, F., Kraft, B., Weber, U., Novick, K., ... & Jung, M. X-BASE: the first terrestrial carbon and water flux products from an extended data-driven scaling framework, FLUXCOM-X. Biogeosciences, 21(22), 5079-5115, 2024, https://doi.org/10.5194/bg-21-5079-2024

Olin, S., Schurgers, G., Lindeskog, M., Wårlind, D., Smith, B., Bodin, P., et al. (2015). Modelling the response of yields and tissue C : N to changes in atmospheric CO2 and N management in the main wheat regions of western Europe. Biogeosciences, 12(8), 2489–2515. https://doi.org/10.5194/bg-12-2489-2015

Olin, S., Lindeskog, M., Pugh, T. A. M., Schurgers, G., Wårlind, D., Mishurov, M., et al. (2015). Soil carbon management in large-scale Earth system modelling: Implications for crop yields and nitrogen leaching. Earth System Dynamics, 6(2), 745–768. https://doi.org/10.5194/esd-6-745-2015

Parton, W. J., Scurlock, J. M. O., Ojima, D. S., Gilmanov, T. G., Scholes, R. J., Schimel, D. S., et al. (1993). Observations and modeling of biomass and soil organic matter dynamics for the grassland biome worldwide. Global Biogeochemical Cycles, 7(4), 785–809. https://doi.org/10.1029/93GB02042

This project has received funding from the European Union's Horizon Europe research and innovation programme under grant agreement No 101081395

Parton, W. J., Schimel, D. S., Cole, C. V., & Ojima, D. S. (1987). Analysis of factors controlling soil organic matter levels in Great Plains grasslands. Soil Science Society of America Journal, 51(5), 1173, https://doi.org/10.2136/sssaj1987.03615995005100050015x

Poeplau, C., & Don, A. (2015). Carbon sequestration in agricultural soils via cultivation of cover crops - A meta-analysis. Agriculture, Ecosystems and Environment, 200, 33–41. https://doi.org/10.1016/j.agee.2014.10.024

Portmann, F. T., Siebert, S., & Döll, P. (2010). MIRCA2000-Global monthly irrigated and rainfed crop areas around the year 2000: A new high-resolution data set for agricultural and hydrological modeling. Global Biogeochemical Cycles, 24(1), 1–24. https://doi.org/10.1029/2008gb003435

Porwollik, V., Rolinski, S., Heinke, J., & Müller, C. (2019). Generating a rule-based global gridded tillage dataset. Earth System Science Data, 11, 823–843. https://doi.org/10.5194/essd-11-823-2019

Pucher, C., Neumann, M., & Hasenauer, H. (2022). An Improved Forest Structure Data Set for Europe. Remote Sensing, 14(2). https://doi.org/10.3390/rs14020395

Qiu, C., Zhu, D., Ciais, P., Guenet, B., Peng, S., Krinner, G., ... & Hastie, A. (2019). Modelling northern peatland area and carbon dynamics since the Holocene with the ORCHIDEE-PEAT land surface model (SVN r5488). Geoscientific Model Development, 12(7), 2961-2982, https://doi.org/10.5194/gmd-12-2961-2019

Quemada, M., Lassaletta, L., Leip, A., Jones, A., & Lugato, E. (2020). Integrated management for sustainable cropping systems: Looking beyond the greenhouse balance at the field scale. Global Change Biology, 26(4), 2584–2598. https://doi.org/10.1111/gcb.14989

Raoult, N., Douglas, N., MacBean, N., Kolassa, J., Quaife, T., Roberts, A. G., ... & Zobitz, J. (2025). Parameter estimation in land surface models: Challenges and opportunities with data assimilation and machine learning. Journal of Advances in Modeling Earth Systems, 17(11), https://doi.org/10.1029/2024MS004733

Rochester, I. J. (2003). Estimating nitrous oxide emissions from flood-irrigated alkaline grey clays. Australian Journal of Soil Research, 41(2), 197–206. https://doi.org/10.1071/SR02068

Salmon, E., Jégou, F., Guenet, B., Jourdain, L., Qiu, C., Bastrikov, V., ... & Ziemblińska, K. (2022). Assessing methane emissions for northern peatlands in ORCHIDEE-PEAT revision 7020. Geoscientific Model Development, 15(7), 2813-2838, https://doi.org/10.5194/gmd-15-2813-2022.

Sitch, S., O'sullivan, M., Robertson, E., Friedlingstein, P., Albergel, C., Anthoni, P., ... & Zaehle, S. (2024). Trends and drivers of terrestrial sources and sinks of carbon dioxide: An overview of the TRENDY project. Global Biogeochemical Cycles, 38(7), e2024GB008102

Smith, B., Wårlind, D., Arneth, A., Hickler, T., Leadley, P., Siltberg, J., & Zaehle, S. (2014). Implications of incorporating N cycling and N limitations on primary production in an individual-based dynamic vegetation model. Biogeosciences, 11(7), 2027–2054. https://doi.org/10.5194/bg-11-2027-2014

Smith, P., Calvin, K., Nkem, J., Campbell, D., Cherubini, F., Grassi, G., et al. (2020). Which practices co-deliver food security, climate change mitigation and adaptation, and combat land degradation and desertification? Global Change Biology, 26(3), 1532–1575. https://doi.org/10.1111/gcb.14878

Susiluoto, J., Raivonen, M., Backman, L., Laine, M., Makela, J., Peltola, O., Vesala, T., and Aalto, T.: Calibrating the sqHIMMELI v1.0 wetland methane emission model with hierarchical modeling and adaptive MCMC, Geoscientific Model Development, 11, 1199–1228, https://doi.org/10.5194/gmd-11-1199-2018, 2018.

This project has received funding from the European Union's Horizon Europe research and innovation programme under grant agreement No 101081395

Tian, H., Yang, J., Lu, C., Xu, R., Canadell, J. G., Jackson, R. B., et al. (2018). The global N2O model intercomparison project. Bulletin of the American Meteorological Society, 99(6), 1231–1251. https://doi.org/10.1175/BAMS-D-17-0212.1

Tian, H., Bian, Z., Shi, H., Qin, X., Pan, N., Lu, C., et al. (2022). History of anthropogenic Nitrogen inputs (HaNi) to the terrestrial biosphere: a 5 arcmin resolution annual dataset from 1860 to 2019. Earth System Science Data, 14(10), 4551–4568. https://doi.org/10.5194/essd-14-4551-2022

Val Martin, M., Blanc-Betes, E., Ming Fung, K., Kantzas, E. P., Kantola, I. B., Chiaravalloti, I., et al. (2023). Improving nitrogen cycling in a land surface model (CLM5) to quantify soil N2O, NO and NH3 emissions from enhanced rock weathering with croplands. Geosci. Model Dev., (16), 5783–5801. https://doi.org/10.5194/gmd-16-5783-2023

Vuichard, N., Messina, P., Luyssaert, S., Guenet, B., Zaehle, S., Ghattas, J., ... & Peylin, P. (2019). Accounting for carbon and nitrogen interactions in the global terrestrial ecosystem model ORCHIDEE (trunk version, rev 4999): Multi-scale evaluation of gross primary production. Geoscientific Model Development, 12(11), 4751-4779, https://doi.org/10.5194/gmd-9-857-2016.

Wagena, M. B., Bock, E. M., Sommerlot, A. R., Fuka, D. R., & Easton, Z. M. (2017). Development of a nitrous oxide routine for the SWAT model to assess greenhouse gas emissions from agroecosystems. Environmental Modelling and Software, 89, 131–143. https://doi.org/10.1016/j.envsoft.2016.11.013

Waha, K., Van Bussel, L. G. J., Müller, C., & Bondeau, A. (2012). Climate-driven simulation of global crop sowing dates. Global Ecology and Biogeography, 21(2), 247–259. https://doi.org/10.1111/j.1466-8238.2011.00678.x

Wang, T., Ottlé, C., Boone, A., Ciais, P., Brun, E., Morin, S., ... & Peng, S. (2013). Evaluation of an improved intermediate complexity snow scheme in the ORCHIDEE land surface model. Journal of Geophysical Research: Atmospheres, 118(12), 6064-6079, https://doi.org/10.1002/jgrd.50395

Wang, F., Cheruy, F., & Dufresne, J. L. (2016). The improvement of soil thermodynamics and its effects on land surface meteorology in the IPSL climate model. Geoscientific Model Development, 9(1), 363-381, https://doi.org/10.5194/gmd-9-363-2016

Wårlind, D., Smith, B., Hickler, T., & Arneth, A. (2014). Nitrogen feedbacks increase future terrestrial ecosystem carbon uptake in an individual-based dynamic vegetation model. Biogeosciences, 11(21), 6131–6146. https://doi.org/10.5194/bg-11-6131-2014

Weier, K. L., Doran, J. W., Power, J. F., & Walters, D. T. (1993). Denitrification and the Dinitrogen/Nitrous Oxide Ratio as Affected by Soil Water, Available Carbon, and Nitrate. Soil Science Society of America Journal, 57(1), 66–72. https://doi.org/10.2136/sssaj1993.03615995005700010013x

Winkler, K., Fuchs, R., Rounsevell, M., & Herold, M. (2021). Global land use changes are four times greater than previously estimated. Nature Communications, 12, 2501. https://doi.org/10.1038/s41467-021-22702-2

Xu-Ri, & Prentice, I. C. (2008). Terrestrial nitrogen cycle simulation with a dynamic global vegetation model. Global Change Biology, 14(8), 1745–1764. https://doi.org/10.1111/j.1365-2486.2008.01625.x

Yangjin, D., Wu, X., Bai, H., & Gu, J. (2021). A meta-analysis of management practices for simultaneously mitigating N2O and NO emissions from agricultural soils. Soil and Tillage Research, 213, 105142. https://doi.org/10.1016/j.still.2021.105142

Yin, X., & Struik, P. C. (2009). C3 and C4 photosynthesis models: An overview from the perspective of crop modelling. NJAS-Wageningen Journal of Life Sciences, 57(1), 27-38, https://doi.org/10.1016/j.njas.2009.07.001Get rights and content

This project has received funding from the European Union's Horizon Europe research and innovation programme under grant agreement No 101081395

Zaehle, S., & Friend, A. D. (2010). Carbon and nitrogen cycle dynamics in the O-CN land surface model: 1. Model description, site-scale evaluation, and sensitivity to parameter estimates. Global Biogeochemical Cycles, 24(1), 1–13. https://doi.org/10.1029/2009GB003521

Zhang, B., Zhou, M., Zhu, B., Kemmann, B., Pfülb, L., Burkart, S., et al. (2023). Threshold-like effect of soil NO3− concentrations on denitrification product N2O/(N2O+N2) ratio is mediated by soil pH. Soil Biology and Biochemistry, 187, 109213. https://doi.org/10.1016/j.soilbio.2023.109213

This project has received funding from the European Union's Horizon Europe research and innovation programme under grant agreement No 101081395

https://eyeclima.eu

BRUSSELS, 26 02 2026

Funded by the European Union. Views and opinions expressed are however those of the author(s) only and do not necessarily reflect those of the European Union. Neither the European Union nor the granting authority can be held responsible for them.

This project has received funding from the European Union's Horizon Europe research and innovation programme under grant agreement No 101081395